frontiers | Frontiers in Astronomy and Space Sciences

TYPE Original Research
PUBLISHED 06 February 2023
DOI 10.3389/fspas.2023.1071743

OPEN ACCESS

EDITED BY
Alvaro De La Cruz-Dombriz,
University of Cape Town, South Africa

REVIEWED BY
Christian Corda,
B. M. Birla Science Centre, India
Demosthenes Kazanas,
Goddard Space Flight Center (NASA),
United States

*CORRESPONDENCE
Václav Vavryčuk,
vv@ig.cas.cz

SPECIALTY SECTION
This article was submitted to Cosmology, a section of the journal Frontiers in Astronomy and Space Sciences

RECEIVED 16 October 2022
ACCEPTED 11 January 2023
PUBLISHED 06 February 2023

CITATION
Vavryčuk V (2023), Gravitational orbits in the expanding Universe revisited.
Front. Astron. Space Sci. 10:1071743.
doi: 10.3389/fspas.2023.1071743

Gravitational orbits in the expanding Universe revisited

Václav Vavryčuk*

Institute of Geophysics, Czech Academy of Sciences, Prague, Czechia

Modified Newtonian equations for gravitational orbits in the expanding Universe indicate that local gravitationally bounded systems like galaxies and planetary systems are unaffected by the expansion of the Universe. This result is derived for the space expansion described by the standard FLRW metric. In this paper, the modified Newtonian equations are derived for the space expansion described by the conformal cosmology (CC) metric. In this metric, the comoving and proper times are different similarly as the comoving and proper distances. As shown by Vavryčuk (Front. Phys. 2022), this metric is advantageous, because it properly predicts the cosmic time dilation, and fits the Type Ia supernova luminosity observations with no need to introduce dark energy. Surprisingly, the solution of the equations for gravitational orbits based on the CC metric behaves quite differently than that based on the FLRW metric. In contrast to the common opinion that local systems resist the space expansion, they expand according to the Hubble flow in the CC metric. The evolution of the local systems with cosmic time is exemplified on numerical modelling of spiral galaxies. The size of the spiral galaxies grows consistently with observations and a typical spiral pattern is well reproduced. The theory predicts flat rotation curves without an assumption of dark matter surrounding the galaxy. The theory resolves challenges to the ΛCDM model such as the problem of faint satellite galaxies, baryonic Tully-Fisher relation or the radial acceleration relation. Furthermore, puzzles in the solar system are successfully explained such as the Faint young Sun paradox or the Moon's and Titan's orbit anomalies.

KEYWORDS

cosmological redshift, cosmic time dilation, conformal metric, dark energy, rotation curves, dark matter, winding problem, galaxy expansion

1 Introduction

Observations of the cosmological redshift interpreted by Lemaître (1927) and Hubble (1929) as an effect of the expansion of the Universe started a new era of cosmology and opened space for applying theory of General Relativity (GR) to cosmological problems. Subsequently, the Friedmann equations (Friedmann, 1922) became the basic equations describing the expanding history of the Universe. Immediately, cosmology was faced with the following fundamental questions: How does the global expansion of the Universe affect local gravitational systems? How do local gravitational fields interact with the expansion and where is a size threshold between systems affected by and resisting the global expansion? Do galaxies and galaxy clusters expand or not? How does the global expansion affect our solar system? These theoretical problems paid attention of many cosmologists, because they have essential consequences for understanding the evolution of the Universe and for interpreting cosmological observations (McVittie, 1933; Einstein and Straus, 1945; Dicke and Peebles, 1964; Noerdlinger and Petrosian, 1971; Carrera and Giulini, 2010; Nandra et al., 2012).

The simplest problem is to study the Newtonian equations of motion for two-point particles placed in the expanding space and mutually attracted by the gravitational force. If the local gravitational field is weak and velocities of particles are non-relativistic, the problem can be solved by perturbations (McVittie, 1933; Noerdlinger and Petrosian, 1971; Bolen et al., 2001; Faraoni and Jacques, 2007). In this case, we assume that the metric of the space expansion is perturbed by a weak gravitational field. Assuming that the space expansion is described by the Friedmann-Lemaitre-Robertson-Walker (FLRW) metric, the metric tensor $g_{\mu\nu}$ of a gravitational field produced by a point mass M situated in the expanding space reads (Noerdlinger and Petrosian, 1971, their Eq. 11).

$$ds^2 = -c^2(1+2\alpha)\,dt^2 + a^2(t)\left((1-2\alpha)\frac{dr^2}{1-kr^2} + r^2 d\Omega^2\right), \qquad d\Omega^2 = d\theta^2 + \sin^2\theta\, d\phi^2, \tag{1}$$

where t is time, c is the speed of light, $a(t)$ is the scale factor, k is the Gaussian curvature of the space, r is the comoving distance, and θ and ϕ are the spherical angles. Parameter

$$\alpha = -\frac{GM}{rc^2},\ |\alpha| \ll 1, \tag{2}$$

is the Newtonian gravitational potential normalized to c^2, and G is the gravitational constant. Assuming a massive non-relativistic particle ($v \ll c$) orbiting in the gravitational field and using the geodesic equation, we finally obtain the following equation for the proper radius R of the orbit (Carrera and Giulini, 2010, their Eq. 12a, b).

$$\ddot{R} = -\frac{GM}{R^2} + \frac{L^2}{R^3} + \frac{\ddot{a}}{a}R, \tag{3}$$

$$L = \text{const}, \tag{4}$$

where $L = RV^{\phi}$ is the proper angular momentum, and V^{ϕ} is the proper tangential velocity. For a more detailed derivation, see **Appendix A**.

Eqs. **3**, **4** are called the modified (or improved) Newtonian equations and they differ from the standard Newtonian equations describing the Kepler orbits by term $\frac{\ddot{a}}{a}R$ in Eq. **3** related to the space expansion. The analysis of the modified Newtonian equations applied to the galaxy dynamics shows that the expansion term $\frac{\ddot{a}}{a}R$ affects the orbits within galaxies negligibly (Faraoni and Jacques, 2007). This result led to the conclusion that galaxies and all smaller gravitational systems are not affected by the space expansion and behave as in the static Universe (Dicke and Peebles, 1964; Noerdlinger and Petrosian, 1971; Cooperstock et al., 1998; Faraoni and Jacques, 2007; Iorio, 2013).

The key in deriving the modified Newtonian equations is the assumption that the space expansion is described by the FLRW metric. However, this metric is not the only metric, which can describe the evolution of the isotropic homogeneous Universe. A potentially applicable metric is also the conformal cosmology (CC) metric (Endean, 1994; Endean, 1997; Ibison, 2007; Kastrup, 2008; Dabrowski et al., 2009; Grøn and Johannesen, 2011; Visser, 2015; Harada et al., 2018). This metric has the scale factor $a(t)$ not only at the space components but also at the time component of the metric tensor $g_{\mu\nu}$. Hence, the metric is characterized not only by the space expansion but also by the time dilation during the cosmic evolution. The CC metric has exceptional properties being intensively studied in GR and its modifications such as the Conformal Gravity theory (Mannheim, 1990; Mannheim, 2006; Mannheim, 2012). Interestingly, the CC metric is Lorentz invariant and leaves the Maxwell's equations unchanged from their form in the Minkowski spacetime (Infeld and Schild, 1945; Infeld and Schild, 1946; Ibison, 2007).

Importantly, Vavryčuk (2022a) shows that the CC metric should be preferable against the FLRW metric, because the FLRW metric is actually inconsistent with observations of the cosmological redshift and cosmic time dilation. He claims that the CC metric is necessary for a proper description of the expansion of the Universe, because: 1) The time-time component of the metric tensor g_{00} must vary with cosmic time similarly as the space-space components, and 2) the comoving and proper times must be different in analogy to the comoving and proper distances. Consequently, time should not be invariant as in the FLRW metric, but its rate must vary during the evolution of the Universe. Without changing the time rate, the frequency of photons propagating in the Universe cannot be changed during the expansion and the photons cannot be redshifted.

The varying time rate during the evolution of the Universe is also supported by observations of Type Ia supernovae (SNe Ia). Since the SNe Ia display rather uniform light curves, they can serve as the standard candles as well as the standard local clocks. The spectral evolution of the light curves and stretching of time in the observer frame was disclosed by many authors (Leibundgut et al., 1996; Goldhaber et al., 1997; Phillips et al., 1999; Goldhaber et al., 2001). The stretching of light curves at high redshift is firmly acknowledged and corrections for time dilation are now routinely applied to the SNe Ia data (Leibundgut, 2001; Goobar and Leibundgut, 2011). The light curve stretching is commonly interpreted as the effect of the cosmic time dilation even though the standard FLRW metric does not allow it.

In addition, the CC model fits the SNe Ia luminosity observations with no need to introduce dark energy and an accelerated expansion of the Universe (Behnke et al., 2002; Vavryčuk, 2022a). A possibility that the varying time rate might solve the dark energy problem is reported also by Visser (2015). Considering the varying time rate during the cosmic evolution has also other important consequences. For example, the cosmological and gravitational redshifts are calculated from the metric tensor by the same formula. This emphasizes a common physical origin of both redshifts. The gravitational redshift reflects the time distortion due to the presence of the local gravitational field, while the cosmological redshift is due to changes of the global gravitational field of the Universe.

Obviously, we can ask a question, whether does a local gravitational field in the CC metric behave differently from that in the FLRW metric or not. Hence, the aim of this paper is to study local gravitational systems in the expanding space described by the CC metric. The gravitational field is assumed to be a perturbation of the global gravitational field of the Universe and velocities of particles are non-relativistic. The improved Newtonian equations are derived using the geodesic equation. It is shown that the local gravitational systems behave quite differently in the CC metric than in the FLRW metric. In contrast to the common opinion that local systems resist the space expansion, the results show that all local systems expand according to the Hubble flow in the CC metric. The evolution of the local systems is exemplified on numerical modelling of spiral galaxies. The presented theory predicts flat rotation curves and the observed morphology of spirals. Also, other observations supporting the presented theory are discussed.

2 Theory

2.1 Expanding Universe described by the CC metric

Let us assume an expanding Universe described by the CC metric in the following form (Grøn and Johannesen, 2011; Vavryčuk, 2022a):

$$\begin{aligned} ds^2 &= a^2(t)\left(-c^2dt^2+\frac{dr^2}{1-kr^2}+r^2d\Omega^2\right),\\ d\Omega^2 &= d\theta^2+\sin^2\theta\, d\phi^2, \end{aligned} \tag{5}$$

where $a(t)$ is the scale factor defining the cosmic expansion, t is the comoving (contravariant) time, c is the speed of light, k is the Gaussian curvature of the space, r is the comoving (contravariant) distance, and θ and ϕ are the spherical angles.

To avoid confusions, we have to discuss the CC metric described by Eq. 5 in more detail. This form of the metric is often used in cosmology but in a modified notation and in a different physical context. Time t is called the "conformal time" and it is usually denoted as η. However, the physical meanings of the comoving time t and the conformal time η are essentially different. Here, we consider time t in Eq. 5 as the physical comoving cosmic time. Consequently, the time-time component of the metric tensor g_{00} is time dependent. The rate of time varies and Eq. 5 encompasses the space expansion as well as the time dilation during the evolution of the Universe. By contrast, the conformal time η is commonly assumed to be a rescaled proper time with no physical meaning and no effects on the metric. The g_{00} component is still time independent as for the FLRW metric. In this way, the metric with the conformal time η describes the space expansion with a uniform rate of time and no time dilation during the evolution of the Universe.

When introducing the FLRW metric, it is often argued that g_{00} can be assumed to be time invariant, because we have a freedom to rescale time to keep g_{00} constant (Weinberg, 1972). From this point of view, the FLRW and CC metrics would be equivalent (Visser, 2015). However, this is not correct, because we cannot rescale arbitrarily a cosmological coordinate system without physical consequences. A trivial example is a relation between the space metrics for a static and expanding Universe. Both metrics can be transformed each into the other. However, this does not mean that the model of the static and expanding Universe are physically equivalent. Similarly, the CC metric and the FLRW metric are not physically equivalent, because the FLRW metric is characterized by a uniform rate of time, but the CC metric is characterized by a varying rate of time during the evolution of the Universe.

2.2 Comoving and proper speeds in the CC metric

Using Eq. 5, the equation of the null geodesics, which describes propagation of photons, $ds^2=0$, reads

$$\begin{aligned} a^2(t)\left(-c^2dt^2+dl^2\right)&=0,\\ dl^2&=\frac{dr^2}{1-kr^2}+r^2d\Omega^2. \end{aligned} \tag{6}$$

Consequently, we get for the comoving velocity v and the proper velocity V of photons (Vavryčuk, 2022a, his Eq. A6)

$$v=\frac{dl}{dt}=c,\quad V=ac. \tag{7}$$

The propagation velocity of massive particles is described by the geodesic equation

$$\frac{d^2x^\mu}{ds^2}+\Gamma^\mu_{\alpha\beta}\frac{dx^\alpha}{ds}\frac{dx^\beta}{ds}=0. \tag{8}$$

Substituting the distance element ds by the time element dt, we obtain

$$\frac{d^2x^\mu}{dt^2}=-\Gamma^\mu_{\alpha\beta}\frac{dx^\alpha}{dt}\frac{dx^\beta}{dt}+\Gamma^0_{\alpha\beta}\frac{dx^\alpha}{dt}\frac{dx^\beta}{dt}\frac{dx^\mu}{dt}. \tag{9}$$

Considering the metric tensor $g_{\mu\nu}$ needed for calculating the Christoffel symbols $\Gamma^\mu_{\alpha\beta}$ in Eq. 9 defined by Eq. 5, we get

$$ac^2\dot{v}+\dot{a}c^2v-\dot{a}v^3=0, \tag{10}$$

hence

$$\frac{\dot{v}}{v\left(1-v^2/c^2\right)}=-\frac{\dot{a}}{a}. \tag{11}$$

Consequently, for a massive non-relativistic particle ($v\ll c$) we write

$$\frac{\dot{v}}{v}=-\frac{\dot{a}}{a} \tag{12}$$

and the comoving velocity v and the proper velocity V read

$$v=v_0a^{-1},\quad V=av=V_0, \tag{13}$$

where subscript "0" refers to quantities at present.

Hence, the proper velocity of photons is not constant as in the FLRW metric, but it increases in the CC metric with the expansion as $a(t)c$, where c is the speed of light for $a=1$. By contrast, the proper velocity of massive non-relativistic particles is not affected by the Universe expansion. This is in contradiction with behaviour of non-relativistic massive particles in the FLRW metric, where the comoving velocity v depends on a as a^{-2} and the proper velocity V as a^{-1}.

Note that the varying speed of light in Eq. 7 for the CC metric is an inevitable consequence of the time dependence of g_{00}. The varying speed of light seems apparently against the basic principles of theory of the Special and General Relativity, but according to Einstein (1920): "The law of the constancy of the velocity of light *in vacuo*, which constitutes one of the fundamental assumptions in the special theory of relativity and to which we have already frequently referred, cannot claim any unlimited validity"..."its results hold only so long as we are able to disregards the influences of gravitational fields on the phenomena (e.g., of light)". Since we do not study the speed of light in free-falling inertial systems but in non-inertial systems, the acceleration due to gravity is not cancelled with the gravitational field. Hence, the varying (coordinate-dependent) speed of light in the CC metric is fully consistent with GR being analogous, for example, to the varying (coordinate-dependent) speed of light known in the famous Schwarzschild solution (Weinberg, 1972).

2.3 Conformal Friedmann equations

Assuming the FLRW metric described by Eq. A-1, the Friedmann equation for the perfect isotropic fluid reads (Peacock, 1999; Ryden, 2016)

$$\left(\frac{a'}{a}\right)^2=\frac{8\pi G}{3}\rho-\frac{kc^2}{a^2}, \tag{14}$$

where $a' = da/dT$ is the derivative of the scale factor $a(t)$ with respect to the proper time T, G is the gravitational constant, ρ is the mean mass density, and k is the spatial curvature of the Universe at present.

In order to express Eq. 14 in the CC metric, we have to substitute the proper time T by the comoving time t and time derivative $a' = da/dT$ by $\dot{a} = da/dt = aa'$. Hence, the conformal Friedmann equation reads

$$\left(\frac{\dot{a}}{a}\right)^2 = \frac{8\pi G}{3}\rho a^2 - kc^2, \tag{15}$$

where $\dot{a}$ denotes the derivative with respect to the comoving time t. Considering the matter-dominated Universe, we get

$$\frac{8\pi G}{3}\rho = H_0^2\,\Omega_m a^{-3}. \tag{16}$$

Eq. 15 is rewritten as (Vavryčuk, 2022a)

$$H^2(a) = H_0^2\left(\Omega_m a^{-1} + \Omega_k\right) \tag{17}$$

with the condition

$$\Omega_m + \Omega_k = 1, \tag{18}$$

where $H(a) = \dot{a}/a$ is the Hubble parameter, H_0 is the Hubble constant, Ω_m is the normalized matter density, and Ω_k is the normalized space curvature. As shown in Vavryčuk (2022a), Eq. 17 describes the Type Ia supernova (SNe Ia) dimming well with no need to introduce dark energy, which is necessary in the standard ΛCDM model in order to fit the SNe Ia data.

Considering $a = 1/(1+z)$, the comoving time t is expressed from Eq. 17 as a function of redshift as follows

$$dt = \frac{1}{H_0(1+z)}\left[\Omega_m(1+z) + \Omega_k\right]^{-1/2} dz, \tag{19}$$

and the proper time T related to comoving t as $dT = a(t)dt$ reads

$$dT = \frac{1}{H_0(1+z)^2}\left[\Omega_m(1+z) + \Omega_k\right]^{-1/2} dz. \tag{20}$$

These relations are needed for relating observations of redshift to cosmic time.

2.4 Gravitational orbits in the expanding Universe

Next, we study the influence of the expanding Universe on the local gravity field produced by a point mass. The gravity field is assumed to produce a small perturbation of the metric tensor $g_{\mu\nu}$ describing the expanding space. So far, this problem has been studied under the assumption that the space expansion is defined by the standard FLRW metric (Carrera and Giulini, 2010), see **Appendix A**. Here, we derive equations for the gravitational orbits for the space expansion defined by the CC metric.

The homogeneous and isotropic expanding space characterized by the CC metric will be disturbed by a spherically symmetric gravitational field produced by a point mass M situated in the origin of coordinates. Since we limit ourselves to the weak gravitational effects of the point mass only, Eq. 5 is modified as follows

$$ds^2 = a^2(t)\left[-c^2(1+2\alpha)\,dt^2 + (1-2\alpha)\frac{dr^2}{1-kr^2} + r^2 d\Omega^2\right], \tag{21}$$

where

$$\alpha = -\frac{GM}{rc^2},\ |\alpha| \ll 1 \tag{22}$$

is the Newtonian gravitational potential normalized to c^2, r is the comoving distance of an orbiting particle from the point mass M, and G is the gravitational constant.

Let us assume a massive non-relativistic particle ($v \ll c$) orbiting in the gravitational field in the plane defined by $\theta = 0$. The metric tensor $g_{\mu\nu}$ is defined by Eq. 21. Calculating the Christoffel symbols $\Gamma^{\mu}_{\alpha\beta}$ in Eq. 9, we get

$$\ddot{r} - r\dot{\phi}^2 - \alpha c^2 + \frac{\dot{a}}{a}\dot{r} - \alpha\left(2\dot{\phi}^2 r - 3\frac{\dot{r}^2}{r}\right) - \frac{1}{c^2}\frac{\dot{a}}{a}\dot{r}\left(\dot{r}^2 + \dot{\phi}^2 r^2\right) = 0, \tag{23}$$

$$r\ddot{\phi} + 2\dot{r}\dot{\phi} + \frac{\dot{a}}{a}r\dot{\phi} + 2\alpha\dot{r}\dot{\phi} - \frac{1}{c^2}\frac{\dot{a}}{a}\dot{\phi}\left(\dot{r}^2 + \dot{\phi}^2 r^2\right) = 0, \tag{24}$$

where dots over quantities mean derivatives with respect to the comoving time t. Since $|\alpha| \ll 1$ and $c^2 \gg 1$, terms multiplied by α or by $1/c^2$ in Eqs. 23, 24 can be neglected and we get the following approximate equations

$$\frac{1}{a}\frac{d}{dt}\left(av^r\right) = -\frac{GM}{r^2} + \frac{\left(v^{\phi}\right)^2}{r} = f_g + f_c, \tag{25}$$

$$\frac{1}{a}\frac{d}{dt}\left(arv^{\phi}\right) = 0, \tag{26}$$

where $v^r = \dot{r}$ is the radial comoving velocity, $v^{\phi} = r\dot{\phi}$ is the tangential comoving velocity, and f_g and f_c are the radial gravitational and centrifugal forces in the comoving coordinate system. If we assume that the orbit of the particle is stationary, the radial and centrifugal forces are balanced ($f_g = -f_c$) and the RHS of Eq. 25 equals zero. Consequently, we get

$$av^r = V^r = \text{const}, \tag{27}$$

$$arv^{\phi} = rV^{\phi} = \text{const}, \tag{28}$$

where V^r and V^{ϕ} are the radial and tangential components of the proper velocity V. For a circular orbit in the comoving coordinates, Eqs. 27, 28 are further simplified as

$$V^r = 0,\ V^{\phi} = \text{const}, \tag{29}$$

$$r = \text{const},\ R = aR_0, \tag{30}$$

where subscript "0" refers to the quantity at present.

2.5 Physical consequences for the evolution of local systems

Eq. 30 is surprising and in contradiction to the common opinion that the expansion of the Universe is without any appreciable effect on local gravitational systems (Carrera and Giulini, 2010). This opinion is based on equations for gravitational orbits in an expanding space described by the FLRW metric (see **Appendix A**). The equations were derived by many authors (Dicke and Peebles, 1964; Pachner, 1964;

Callan et al., 1965; Cooperstock et al., 1998; Faraoni and Jacques, 2007; Sereno and Jetzer, 2007; Carrera and Giulini, 2010) and they differ from the standard Newtonian equations for orbits in the static Universe only slightly. The only difference is that the equation for the radial acceleration of an orbiting body in the gravitational field imbedded in the space with the FLRW metric contains a term $\frac{\ddot{a}}{a}R$, which is related to the space expansion (see **Appendix A**, Eq. A-7). It can be shown that this term might be appreciable in dynamics of large-scale structures as galaxy clusters, but the orbits within galaxies are affected negligibly. Consequently, all gravitationally bound systems with size of galaxies or smaller should be unaffected by the space expansion.

By contrast, considering the CC metric for the expanding Universe, the evolution of the local gravitational systems is essentially different from that obtained for the FLRW metric. In particular, the CC metric predicts:

1 An increase of the proper orbital radius $R_{\rm orb}$ with the expansion irrespective of the size of the local system and an increase of the proper orbital period $T_{\rm orb}$ with the expansion. Consequently, the size of galaxies (and all other local gravitational systems) must growth in the expanding Universe. The rate of growth is $(1+z)^{-1}$. The orbit is stationary in comoving coordinates but non-stationary in proper coordinates.
2 A constant proper rotation velocity V^{ϕ} of particles along the orbits irrespective of the orbital radius during the space expansion. Hence, the stationary circular orbits in the comoving coordinate system become spirals in the proper coordinate system. Stars and gas within spirals have flat rotation curves. Since the flat rotation curves are a consequence of the expansion of the Universe, no dark matter is needed to explain dynamics of galaxies.

3 Numerical modelling of the galaxy dynamics

In this section, we will examine the evolution of local gravitationally bounded systems in the expanding Universe by numerical modelling. The modelling is simple and reflects only basic features of the galaxy evolution. It is focused on studying the formation of spirals and their evolution in time. The gravitational field is axially symmetric and interactions between stars and gas inside spirals are neglected. The aim is just to demonstrate the potential of the derived Eqs **29**, **30** of gravitational orbits in the CC metric for the full realistic modelling of the galaxy evolution in future studies.

3.1 Parameters for modelling

For modelling, we need to specify the expanding history of the Universe described by the Hubble parameter $H(z)$. Since we do not use the FLRW metric, we cannot adopt the ΛCDM model. Instead, the CC metric described by Eq. **17** must be used. According to Vavryčuk (2022a), we use parameters $\Omega_m = 1.2$, $\Omega_\Lambda = 0$ (no dark energy), and $\Omega_k = -0.2$ (closed Universe). The Hubble constant is $H_0 = 69.8$ km s^{-1} Mpc^{-1}, obtained by Freedman et al. (2019) from observations of the SNe Ia data with a red giant calibration. Obviously, Eqs. **17**, **19** predict a quite different evolution of the Hubble parameter and a time-redshift relation than the ΛCDM model. For example, redshift $z = 4$ corresponds to the cosmic time of 12 Gyr for the ΛCDM model but 8.2 Gyr for the CC model (see **Figure 1**).

The galaxy is assumed to be formed by a bulge and disk with the following exponential density profiles (McGaugh, 2016)

$$\Sigma_b(R) = \Sigma_b(R_{b0})\, e^{-(r-R_{b0})/R_b}, \tag{31}$$

$$\Sigma_d(R) = \Sigma_d(R_{d0})\, e^{-(r-R_{d0})/R_d}, \tag{32}$$

where $\Sigma_b(R)$ and $\Sigma_d(R)$ are the surface densities of the bulge and disk, respectively. The required parameters are for the bulge $\Sigma_b(R_{b0}) = 3.6$ M$_\odot$ pc^{-2}, $R_{b0} = 2.5$ kpc, $R_b = 0.3$ kpc, and for the disk $\Sigma_d(R_{d0}) = 99.2$ M$_\odot$ pc^{-2}, $R_{d0} = 8.0$ kpc, $R_d = 2.8$ kpc. The total masses of the bulge and disk are $M_b = 8.5 \times 10^9$ M$_\odot$ and $M_d = 8.5 \times 10^{10}$ M$_\odot$, respectively. The bulge is usually modelled as a prolate, triaxial bar (Binney et al., 1997; Bissantz and Gerhard, 2002), but we do not focus on modelling a 3D geometry of the bulge and its evolution, so the simplified approximation described by Eq. **31** is satisfactory.

3.2 Bulge-bar region and spirals

The density profiles and the Newtonian rotation curves predicted for the used parameters are shown in **Figure 2**. The total rotation curve (**Figure 2B**, black line) is separated into two domains. The separation (critical) distance R_c is about 4 kpc (**Figure 2B**, dashed vertical line) and corresponds to the maximum rotation velocity associated with the disk density profile (**Figure 2B**, red line). For shorter distances (bulge-bar domain), the behaviour of the rotation curve is complex being affected by both the bulge and disk. For larger distances (spiral domain), the initial rotation curve is monotonously decreasing affected mostly by the total mass in the bulge-bar area. Obviously, the critical distance R_c may vary for different galaxies being dependent on their mass and density profiles. As discussed below, the rotation curve evolves in time and the final rotation curve becomes flat in the spiral domain (**Figure 2B**, green line).

Figure 3 shows the bulge-bar and spiral regions for the spiral galaxy UGC 6093 together with a scheme suggesting a possible origin of spirals and their temporal evolution. The bulge-bar region is characterized by a high concentration of stars and gas. Consequently, gravitational forces maintain the shape of the galaxy inside this region, irrespective of its rotation. Since the bar is continuously increasing due to the space expansion, its ends cross the region boundary and outflow from the bulge-bar region into the spiral region. In this region, the radial gravitational forces become dominant and stars and gas move as bodies in a spherically symmetric gravitational field. Their motion will be described by Eqs. **29**, **30**: the rotation velocity will be constant with time but the orbital radius will increase. Consequently, the rotating bar will outstrip the material in the spiral region, which will form a pattern of trailing spirals. The material will display flat rotation curves in all spirals, and the size of galaxies will increase with time.

3.3 Scenarios of the galaxy evolution

The form of spirals depends on several factors: 1) The radius of the bulge-bar area, 2) the age of the galaxy, 3) the mass of the galaxy, density profile and its rotation velocity, and 4) the expansion history of

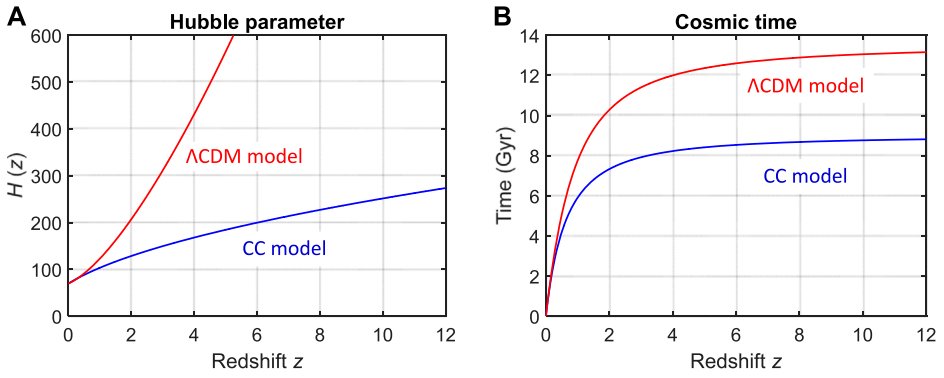

FIGURE 1
The Hubble parameter **(A)** and the proper cosmic lookback time **(B)** as a function of redshift. The cosmological model is described by Eq. **17** for the CC metric (blue line) with $\Omega_m = 1.2$, and $\Omega_k = -0.2$ (Vavryčuk, 2022a). The red line shows the standard ΛCDM model. The Hubble constant is $H_0 = 69.8$ km s^{-1} Mpc^{-1}, obtained by Freedman et al. (2019) from observations of the SNe Ia data with a red giant calibration. Note that panel **(B)** does not imply that the age of the Universe is less than about 9 Gyr in the CC model. For redshifts $z > 15$, the cosmic evolution becomes more complicated due to light-matter interactions, and Eq. **17** must be modified, see Vavryčuk (2022b).

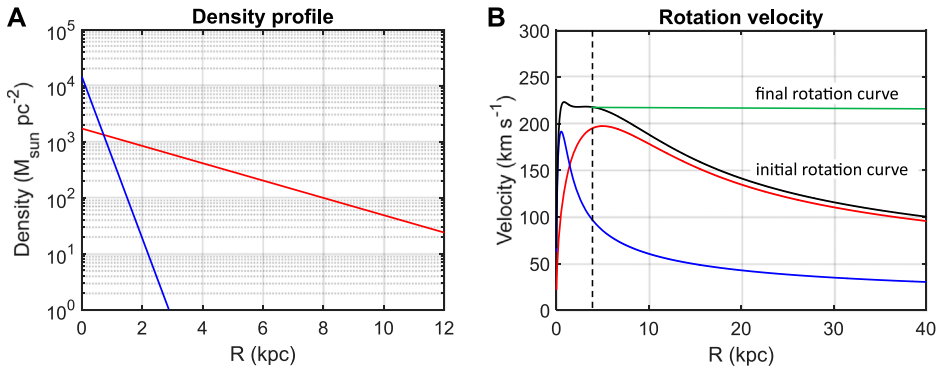

FIGURE 2
The density profile **(A)** and the initial and final rotation velocity curves **(B)** for a simulated galaxy. The surface densities of the bulge (blue line in **(A)**) and disk (red line in **(A)**) are calculated by Eqs **31**, **32** with $\Sigma_b(R_{b0}) = 3.6$ M$_\odot$pc^{-2}, $R_{b0} = 2.5$ kpc, $R_b = 0.3$ kpc for the bulge, and with Σ_d (R_{d0}) = 99.2 M$_\odot$ pc^{-2}, R_{d0} = 8.0 kpc, $R_d = 2.8$ kpc for the disk. The total masses of the bulge and disk are $M_b = 8.5 \times 10^9$ M$_\odot$ and $M_d = 8.5 \times 10^{10}$ M$_\odot$, respectively. The total initial rotation velocity (black line in **(B)**) is shown together with the contribution of the bulge (blue line in **(B)**) and disk (red line in **(B)**). The vertical dashed line in **(B)** defines the boundary $R_c = 4$ kpc between the bulge-bar regime and the trailing-spiral regime. The green line in **(B)** shows the final rotation curve caused by the space expansion (the stellar mass and gas with $R > R_c$ are continuously moving out of the galaxy centre, but they keep their rotation velocity).

the Universe. Therefore, we assume several alternative scenarios in the numerical modelling, where we vary some of these parameters. The radius of the bulge-bar area R_c will be considered 3, 4, and 5 kpc. The age of a galaxy will be 8.0, 8.5, and 8.8 Gyr. This age will correspond to the redshift z of 3.2, 5.6, and 11.2. The masses of the bulge and disk of a galaxy are $M_b = 8.5 \times 10^9$ M$_\odot$ and $M_d = 8.5 \times 10^{10}$ M$_\odot$, but we will also model a galaxy with a half of this mass and with a twice higher mass.

In order to simulate a more realistic galaxy evolution, we assume random conditions for the bulge-bar outflow. The critical distance R_c is not defined by a single value, but it varies according to the Gaussian distribution with the standard deviation of 0.05 kpc. Similarly, the bulge-bar outflow does not cross the domain boundary at two single points defined at the two ends of the bar by angles $\phi = 0°$ and 180°. Instead, angle ϕ obeys the Gaussian distribution centred at 0° and 180° with the standard deviation of 20°.

3.4 Results

In modelling, we calculate orbits of stars and gas flowed out from the bulge-bar domain into the spiral domain and the evolution of the orbits in time. Geometry of orbits is defined by Eqs. **29**, **30**, in which we specify the rotation velocity at the boundary between the bulge-bar and spiral regions and the expansion history defined by the Hubble parameter $H(z)$. **Figure 4** shows the evolution of a galaxy with age of 8.8 Gyr. The galaxy started to evolve at redshift z of 11.2. The galaxy was formed just by the bulge and bar with no spirals at the beginning of the simulation. At this time, the radius of the galaxy was 4 kpc being the same as the radius of the bulge-bar area. The material, which outflowed from the bulge-bar domain due to the space expansion, formed typical trailed spirals during the galaxy evolution (**Figure 4B**). Hence, the radius of the galaxy increased from 4 kpc to 49 kpc during its life (**Figure 4A**). The rotation velocity of the material in the spirals

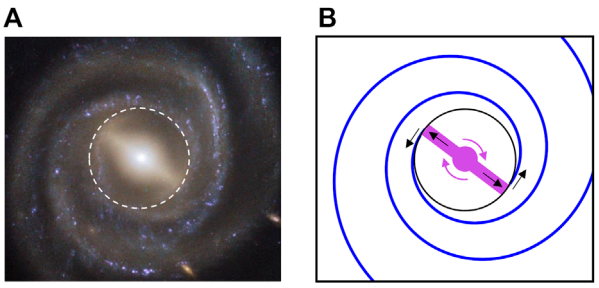

FIGURE 3
The spiral galaxy UGC 6093 observed by ESA/Hubble **(A)** and the scheme of the spiral galaxy **(B)**. The bulge and bar of the galaxy in plot **(B)** is marked by the purple colour. The purple arrows in **(B)** show the rotation direction of the bar. The black arrows in **(B)** show the direction of the outflow from the bulge-bar domain into the spiral domain. The white dashed circle in **(A)** and the solid black circle in **(B)** mark the boundary between the bulge-bar and spiral domains.

is uniform and attains a value of 217.7 km/s. The classical problem in the galaxy dynamics called the "winding paradox" of spirals (Ferreras, 2019) cannot appear, because the radius of spirals is continuously increased and spiral arms are moving away from the bulge-bar region.

Figure 5 demonstrates a dependence of the spiral pattern on the size of the bulge-bar area. The age of the galaxy is again 8.8 Gyr and the evolution started at redshift z of 11.2. For a smaller radius of the bulge-bar area (**Figure 5A**, R_c = 3 kpc), the rotation velocity is slightly higher being 218.3 km/s. As a result, the orbital period is smaller and the recession of the spirals from the central part of the galaxy is not so pronounced. By contrast, for a larger radius of the bulge-bar area (**Figure 5C**, R_c = 5 kpc), the rotation velocity is slightly lower being 215.2 km/s. The orbital period is higher and the recession of the spirals from the central part of the galaxy is more distinct.

Figure 6 shows how is the spiral pattern affected by the age of the galaxy. The figure shows three galaxies with the age of 8.0, 8.5, and 8.8 Gyr. The corresponding redshifts are 3.2, 5.6, and 11.2. The radius of the bulge-bar area is R_c = 4 kpc and the rotation velocity is 217.7 km/s for all three galaxies. As expected, the younger the galaxy, the less evolved the spiral pattern. Consequently, the final radius of the galaxy increased from 4 kpc to 17, 26, and 49 kpc, respectively.

Finally, **Figure 7** presents how is the spiral pattern affected by the mass of a galaxy. **Figure 7B** shows a galaxy with masses of the bulge and disk of a galaxy are $M_b = 8.5\times10^9$ $M_\odot$ and $M_d = 8.5\times10^{10}$ $M_\odot$ (rotation velocity at R_c = 4 kpc is 217.7 km/s). These values were used in all previous simulations (**Figures 4–6**). **Figure 7A** shows a galaxy, which has a twice higher mass. The corresponding rotation velocity at R_c = 4 kpc is 307.9 km/s. By contrast, **Figure 7C** shows a galaxy, which has a twice lower mass. The corresponding rotation velocity at R_c = 4 kpc is 153.9 km/s only. The age of the three galaxies is 8.8 Gyr and their evolution started at redshift z = 11.2. Since the galaxies have the same age, their size increases in the same way: from 4 kpc to 49 kpc. Still the spiral pattern is remarkably different for all three galaxies. The massive galaxy rotates fast and the spirals are receding slowly from the galaxy centre (**Figure 7A**). The galaxy with the smallest mass rotates slowly and the recession of spirals from the galaxy centre is high (**Figure 7C**).

4 Supporting observational evidence

The presented results are supported by many observations difficult to explain under the standard cosmological model. This applies to galaxy dynamics, morphology of spiral galaxies as well as dynamics of the solar system. In the next, we review several puzzles in modern cosmology resolved by the proposed theory.

4.1 Galaxy expansion

As shown in the previous sections, the size of galaxies should increase with redshift as $(1+z)^{-1}$ with no change of the galaxy mass. Based on observations, it is accepted that the size of galaxies evolves rapidly during the cosmic time (van Dokkum et al., 2008; van Dokkum et al., 2010; Williams et al., 2010), see **Figure 8**. Using observations from the Hubble Space Telescope (HST), galaxy sizes defined by the effective radius, R_e, have been extensively measured with the Advanced Camera for Surveys (ACS) and the Wide Field Camera 3/IR channel on board HST for massive galaxies at $z < 3$ (van der Wel et al., 2014) and $z \geq 3$–4 Lyman break galaxies (LBGs) selected in the dropout technique (Trujillo et al., 2006; Dahlen et al., 2007; McLure et al., 2013). The average size is reported to evolve according to $R_e \sim (1+z)^{-B}$, with B ranging most frequently between 0.8 and 1.2 (Bouwens et al., 2004; Oesch et al., 2010; Holwerda et al., 2015). For example, Shibuya et al. (2015) studied the redshift evolution of the galaxy effective radius R_e obtained from the HST samples of ~190,000 galaxies at z = 0–10, consisted of 176,152 photo-z galaxies at z = 0–6 from the 3D-HST + CANDELS catalogue and 10,454 Lyman break galaxies (LBGs) at z = 4–10 identified in the CANDELS, HUDF 09/12, and HFF parallel fields. They found that R_e values at a given luminosity decrease toward high z, as $R_e \sim (1+z)^{-B}$, with $B = 1.10 \pm 0.06$ for median, see **Figure 8A**.

Since it is believed that the size of galaxies cannot be affected by the expansion of the Universe, the observed expansion of galaxies is explained by other mechanisms. The most popular theory suggests the growth of galaxies being produced by galaxy mergers (Naab et al., 2009; Kormendy and Ho, 2013; McLure et al., 2013; Conselice, 2014). An important role in merging of galaxies play dark matter haloes (Kauffmann et al., 1993; Mo et al., 1998). Two types of mergers are distinguished: a major merger where the stellar masses of the galaxies are comparable, and a minor merger where the stellar mass of one galaxy is much lower.

However, the idea of the galaxy expansion due to galaxy mergers is controversial for several reasons (Lerner, 2018). First, observations indicate that the major and minor merger rates are much lower to explain the galaxy expansion (Taylor et al., 2010; Man et al., 2012; Man et al., 2016). For example, Mundy et al. (2017) report approximately 0.5 major mergers at $z < 3.5$ representing an increase in stellar mass of 20%–30% only when considering constant stellar mass samples. As regards minor mergers, Newman et al. (2012) studied 935 galaxies selected with $0.4 < z < 2.5$ and concluded that minor merging cannot account for a rapid growth of the size seen at higher redshifts. Man et al. (2016) studied massive galaxies using the UltraVISTA/COSMOS catalogue, complemented with the deeper, higher resolution 3DHST + CANDELS catalogue and estimated ~1 major merger and ~0.7 minor merger on average for a massive ($M_\star \geq 10^{10.8}$ $M_\odot$) galaxy during z = 0.1–2.5. The observed number of major and minor mergers can increase the size of a massive quiescent

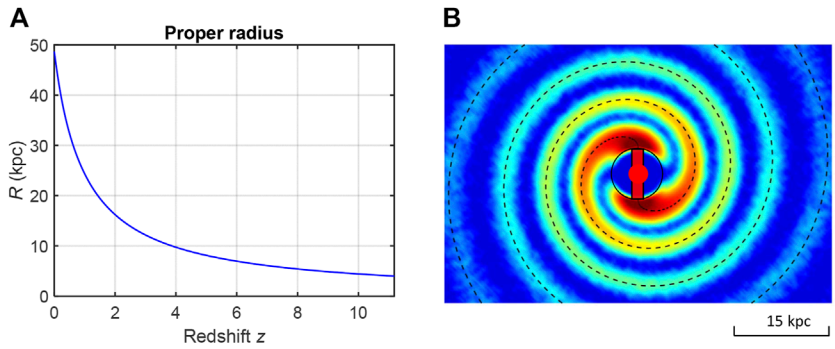

FIGURE 4
The proper radius of a galaxy as a function of redshift **(A)**, and the spiral arms formed during the galaxy evolution **(B)**. The density of the material in the spiral arms in **(B)** is colour coded. The age of the galaxy is 8.8 Gyr and the maximum redshift is $z = 11.2$. The solid black circle in **(B)** marks the boundary between the bulge-bar and spiral domains with radius $R_c = 4$ *kpc*. The black dashed line in **(B)** denotes the central orbit with unperturbed parameters R_c and ϕ. The other orbits forming the spirals are characterized by perturbed parameters R_c and ϕ, see the text. The red bulge and bar inside the black circle in **(B)** illustrate schematically the orientation of the bar.

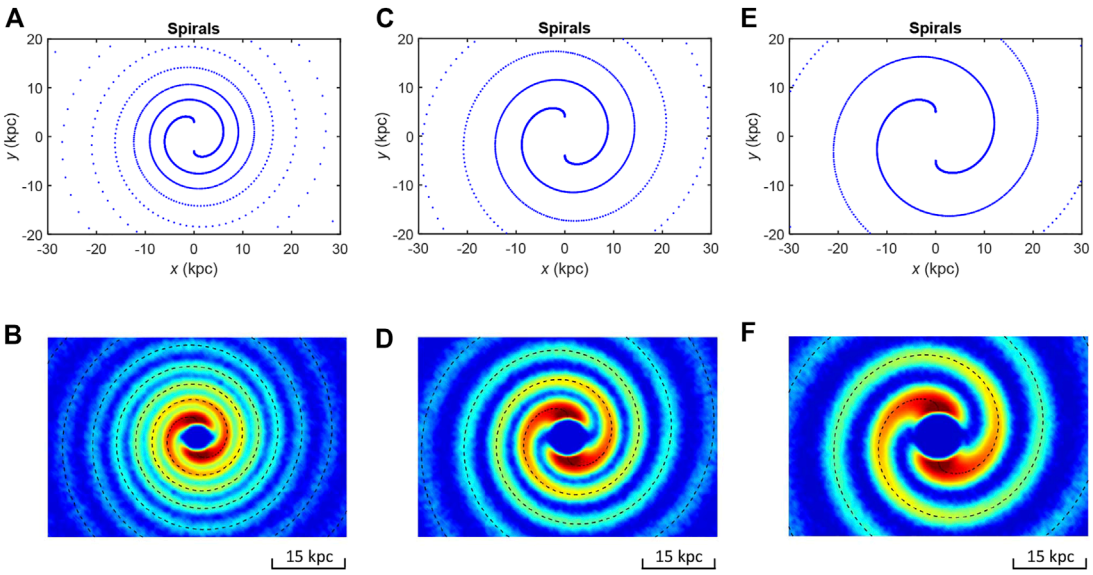

FIGURE 5
Geometry of spirals: dependence on the initial size of the bulge-bar region. The age of the galaxy is 8.8 Gyr and the maximum redshift is $z = 11.2$. The upper/lower plots show orbits with unperturbed/perturbed parameters R_c and ϕ. The critical radius R_c and the rotation velocity V^{ϕ} are 3 kpc and 218.3 km/s in **(A, B)**, 4 kpc and 217.7 km/s in **(C, D)**, and 5 kpc and 215.2 km/s in **(E, F)**. The masses of the bulge and disk are $M_b = 8.5 \times 10^9$ $M_\odot$ and $M_d = 8.5 \times 10^{10}$ $M_\odot$, respectively.

galaxy by a factor of two at most. Hence, additional mechanisms are needed to fully explain the galaxy evolution. Second, mergers cannot explain the growth of spiral galaxies, because mergers destroy disks as shown by Bournaud et al. (2007). Third, the idea of mergers implies an increase of stellar mass in galaxies over cosmic time. However, observations show no or slight mass evolution in time (Bundy et al., 2017; Kawinwanichakij et al., 2020).

4.2 Galaxy rotation curves

Another basic characteristics predicted by the presented theory are flat rotation curves of spiral galaxies. In Newton theory, a velocity of stars in a rotating galaxy is controlled by gravitational and centrifugal forces only. Assuming the Newton's gravitation law, a balance between the forces implies a decay of the orbital speed $V(R)$ of a star with its distance R from the galaxy centre

$$V^2(R) = \frac{GM(R)}{R}, \tag{33}$$

where $M(R)$ is the mass of the galaxy as a function of R. Hence, the rotation curve $V(R)$ decays as $R^{-1/2}$ provided the most of mass is concentrated in the galaxy centre. The same applies to the improved Newtonian equations in an expanding Universe described by the standard FLRW metric. Obviously, the flat rotation curves predicted by the improved Newtonian equations in the Universe with

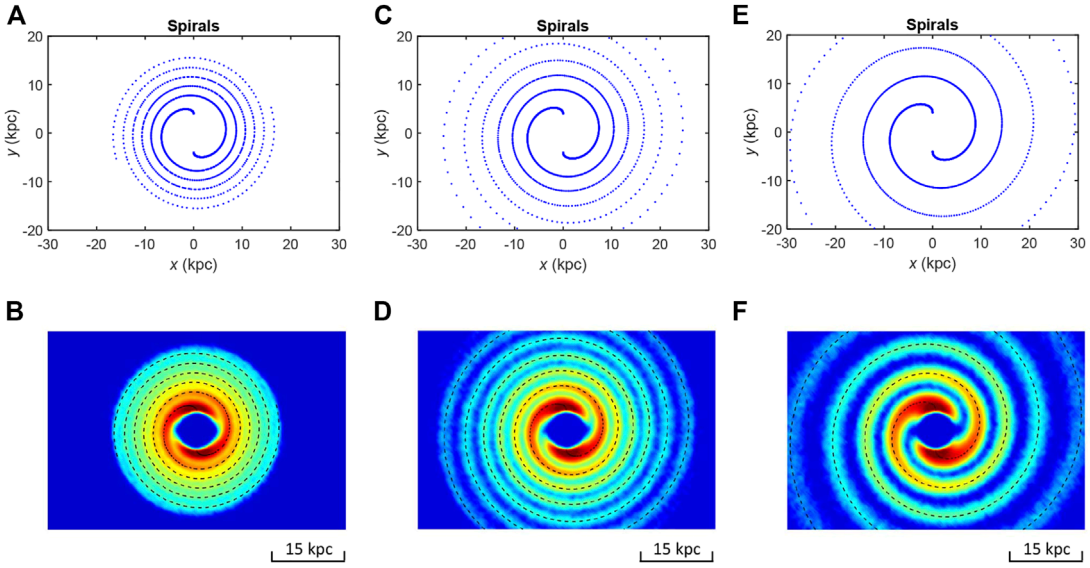

FIGURE 6
Geometry of spirals: dependence on the galaxy age. The critical radius R_c and the rotation velocity V^{ϕ} are 4 kpc and 217.7 km/s. The upper/lower plots show orbits with unperturbed/perturbed parameters R_c and ϕ. The galaxy age and the maximum redshift are 8.0 Gyr and $z = 3.20$ in **(A, B)**, 8.5 Gyr and $z = 5.65$ in **(C, D)**, and 8.8 Gyr and $z = 11.18$ in **(E, F)**. The masses of the bulge and disk are $M_b = 8.5 \times 10^9$ $M_\odot$ and $M_d = 8.5 \times 10^{10}$ $M_\odot$, respectively.

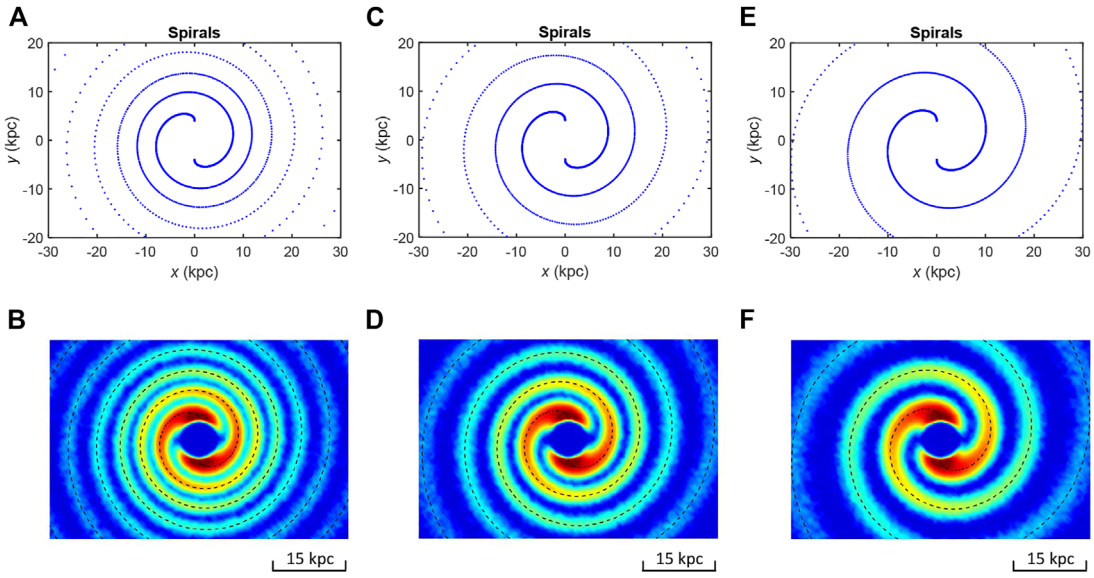

FIGURE 7
Geometry of spirals: dependence on the galaxy mass. The critical radius R_c, the galaxy age and the maximum redshift are 4 kpc, 8.8 Gyr and $z = 11.18$. The upper/lower plots show orbits with unperturbed/perturbed parameters R_c and ϕ. The masses of the bulge and disk are $M_b = 17 \times 10^9$ $M_\odot$ and $M_d = 17 \times 10^{10}$ $M_\odot$ in **(A, B)**, $M_b = 8.5 \times 10^9$ $M_\odot$ and $M_d = 8.5 \times 10^{10}$ $M_\odot$ in **(C, D)**, and $M_b = 4.25 \times 10^9$ $M_\odot$ and $M_d = 4.25 \times 10^{10}$ $M_\odot$ in **(E, F)**. The rotation velocity V^{ϕ} is 307.9 km/s in **(A, B)**, 217.7 km/s in **(C, D)**, and 153.9 km/s in **(E, F)**.

the CC metric point to fundamental differences between both the metrics. Importantly, the flat rotation curves of spiral galaxies are observationally confirmed.

4.2.1 Observations of flat rotation curves

Rubin and Ford (1970) discovered that the rotation curve of the Andromeda Galaxy has a sharp maximum of $V = 225$ km/s at $R = 400$ pc, a deep minimum at $R = 2$ kpc, and it is nearly flat at $R > 3$ kpc with the maximum velocity of 270 ± 10 km/s. Such behaviour was later confirmed also for other spiral galaxies (Rubin et al., 1980; Rubin et al., 1985; van Albada et al., 1985; Begeman, 1989; Sanders, 1996; Swaters et al., 2000; Sofue and Rubin, 2001; de Blok and Bosma, 2002; de Blok et al., 2008; McGaugh, 2019; Tiley et al., 2019), for an example, see the rotation curve of the NGC

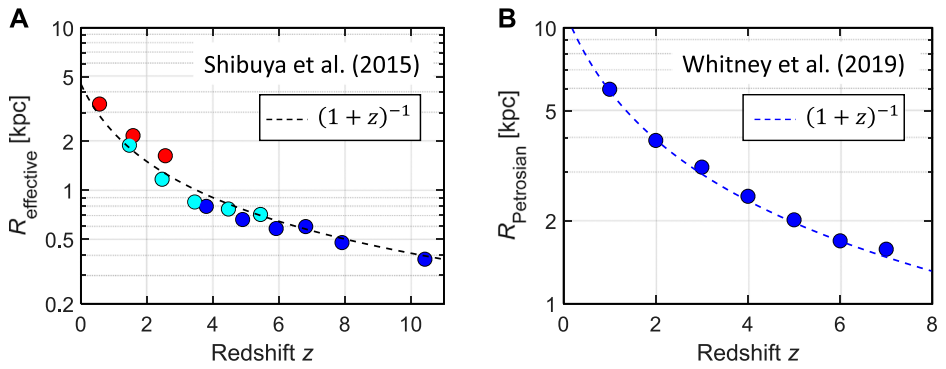

FIGURE 8
Galaxy size evolution with redshift. **(A)** Median of the effective galaxy radius R as a function of redshift for galaxies in the bin of $L_{UV} = (0.3-1)\,L^{*}_{z=3}$. The red and cyan filled circles indicate radius R for star-forming galaxies measured in the optical (4,500–8,000 Å) and UV (1,500–3,000 Å) wavelength ranges, respectively. The blue filled circles indicate radius R for the Lyman break galaxies measured in the UV wavelength range. For details, see Shibuya et al. (2015, their Figure 8). **(B)** Median Petrosian radius of galaxies as a function of redshift for the mass-limited sample in the range of $10^9\ M_\odot \le M^* \le 10^{10.5}\ M_\odot$. The ratio of the surface brightness at radius R to the mean surface brightness of a galaxy is $\eta = 0.2$. For details, see Whitney et al. (2019, their Figure 8). The dashed lines in **(A, B)** show the size evolution predicted by the presented theory.

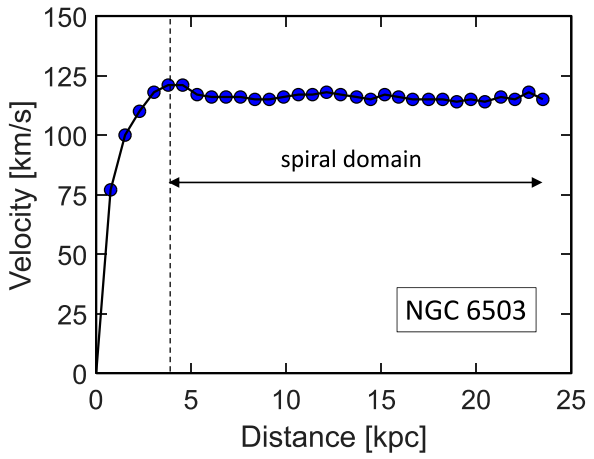

FIGURE 9
Rotation curve for the NGC 6503 Galaxy. The spiral domain covering distances greater than 4 kpc is indicated. In this domain, receding of spirals from the galaxy centre causes the flatness of the rotation curve. For data, see Begeman (1987) and Lelli et al. (2016a).

6503 Galaxy in **Figure 9**. The measurements of rotation curves are mostly based on (Sofue, 2017): observations of emission lines at optical wavelengths such as Hα and [N_{II}] lines, particularly, in H_{II} regions in galactic disks; at infrared wavelengths revealing kinematics of dusty disks and nuclear regions of spiral galaxies with significant dust extinction; and at 21-cm H_I line powerful to study kinematics of entire spiral galaxy.

The rotation curves of spiral galaxies display a significant similarity irrespective of their morphology (Persic et al., 1996; Sofue, 2016; Sofue, 2017). The differences are mainly connected to the mass and size of the galaxies. More massive and larger galaxies (Sa and Sb) have high rotation velocity close to the nucleus, while smaller galaxies (Sc) show slower rotation in the centre. The earlier-type (Sa and Sb) galaxies display a flat or slowly declining velocity at the outermost part of the rotation curve, while the rotation velocity of the later-type (Sc) galaxies monotonically increases. Similarly, dwarf and LSB galaxies display monotonically increasing rotation velocity until their galaxy edges (Swaters et al., 2000; de Blok et al., 2001; Swaters et al., 2003). In addition, Tully and Fisher (1977) revealed an empirical statistical relation between the galaxy luminosity and the maximum rotation velocity at a few galactic disk radii. The Tully-Fisher relation is commonly used for estimating the luminosity of distant galaxies (Jacoby et al., 1992; Mathewson et al., 1992; Phillips, 1993) and for measuring the Hubble constant (Mould et al., 2000; Freedman et al., 2001).

4.2.2 Dark matter

To explain the discrepancy between predicted and observed rotation curves, several theories have been proposed. The most straightforward way is to assume the presence of dark matter (DM) with distribution calculated as (Schneider, 2015, his Eq. 3.17)

$$M_{\rm dark}(R) = \frac{R}{G}\left(V^2_{\rm obs}(R) - V^2(R)\right), \tag{34}$$

where $V_{\rm obs}(R)$ is the observed rotation velocity and $V(R)$ is calculated according to Eq. **33**. The idea of dark matter origins from Zwicky (Zwicky, 1937; Zwicky, 2009) who postulated "missing mass" to account for the orbital velocities of galaxies in clusters. Originally, the DM was assumed to be baryonic formed by gas, dust and microscopic and macroscopic solid bodies including black-holes. Later on, the baryonic origin of DM was questioned and rejected. Since the analysis of galaxy rotation curves revealed that the mass of DM (van Albada et al., 1985; Dubinski and Carlberg, 1991; Navarro et al., 1996; Persic et al., 1996; Navarro et al., 1997) is much higher than estimates of dust and gas in galaxies (Calzetti et al., 2000; Dunne et al., 2000; Draine and Li, 2007; da Cunha et al., 2008; Sandstrom et al., 2013), DM was considered to be mostly of non-baryonic nature (White and Rees, 1978; Davis et al., 1985; White et al., 1987; Maddox et al., 1990; Moore et al., 1999; Bergström, 2000; Bertone and Hooper, 2018). To reconcile the theoretical and observed rotation curves, the DM is significant at large distances and forms a DM halo with the total mass exceeding the stellar galaxy mass by about one order or more (van Albada et al., 1985; Dubinski and Carlberg, 1991; Navarro et al., 1996; Persic et al., 1996).

4.2.3 Conformal Gravity and MOND theory

The non-baryonic DM concept is not, however, unanimously accepted. The non-baryonic DM is questioned, in particular, for its exotic and mysterious nature and for difficulties to be detected by other methods independent of gravity. Also, significant discrepancies with predictions of the ΛCDM model on small scale are reported by many authors (Kroupa, 2015; Del Popolo and Le Delliou, 2017). Therefore, several alternative theories have been proposed to explain the flat rotation curves (Mannheim, 2006). The most famous alternative theories are the Conformal Gravity and Modified Newtonian Dynamics theory (Mannheim, 2006).

The Conformal Gravity (CG) attempts to solve both the problems of dark energy and dark matter. Similarly as the CC approach presented in this paper, the CG theory emphasizes the importance of conformal transformations for solving gravity problems (Mannheim, 2006). However, both the approaches are essentially different: the CC metric is applied to the standard GR equations, while the CG theory is based on modifying the GR equations, in order the equations to be conformally invariant. The CG equations are based on minimizing the Weyl action with the use of the Weyl conformal tensor rather than on the Einstein-Hilbert action (Mannheim, 1990; Mannheim, 2006; Mannheim, 2012). The CG theory avoids dark energy as well as fits rotation curves without use of dark matter. Unlike the Newtonian gravity, the CG is global theory, where both the local galactic and the exterior gravitational fields are considered. The rotation velocity is affected by a linear potential caused by the Hubble flow and by a quadratic potential caused by inhomogeneities (Mannheim and O'Brien, 2011; Mannheim, 2019). As reported by Mannheim (2019), the CG theory has successfully fitted rotation curves of 207 galaxies including dwarf galaxies, see also Mannheim and O'Brien (2012) and O'Brien and Mannheim (2012).

The Modified Newtonian Dynamics (MOND) theory was presented by Milgrom (1983a), Milgrom (1983b), Bekenstein (2004), Milgrom (2010), and Milgrom (2012), who proposed to modify the Newton gravity law for very low accelerations. Below $a_0 \sim cH_0/6$, the standard Newton gravity acceleration g_N is substituted by $\sqrt{a_0 g_N}$. This causes that the Newton's law keeps valid for planetary and other small-scale systems but it does not apply to galaxies and galaxy clusters. As a consequence, rotation curves fit well observations (Begeman et al., 1991). Except for the flat rotation curves, the MOND theory is successful in accounting for some other phenomena listed below, which are difficult to explain using the DM hypothesis (Sanders and McGaugh, 2002; Bugg, 2015).

4.2.3.1 Faint satellite galaxies

The existence of the non-baryonic DM is questioned by a detailed study of properties of faint satellite galaxies of the Milky Way (MW), see Kroupa et al. (2010), which are distributed on a planar structure. Similar alignments were observed also in isolated dwarf galaxies in the local group (Pawlowski and Kroupa, 2013; Pawlowski and McGaugh, 2014) as well as in more distant galaxies (Galianni et al., 2010; Duc et al., 2014). This is a challenge for cosmological simulations, because the DM sub-haloes are assumed to be isotropically distributed.

4.2.3.2 Dual Dwarf Galaxy Theorem

The standard ΛCDM model predicts two types of dwarf galaxies: Primordial DM dominated dwarf galaxies (Type A), and tidal and ram-pressure dwarf galaxies (Type B). While Type A dwarfs should surround the host galaxy spherically, the B dwarfs should be typically correlated in phase space. However, only dwarf galaxies of Type B are observed. This falsifies the Dual Dwarf Galaxy Theorem and the presence of DM haloes (Kroupa, 2012).

4.2.3.3 Baryonic Tully-Fisher relation

Observation of the baryonic Tully-Fisher (BTF) relation, which is a power-law relation between the rotation velocity of a galaxy and its baryonic mass M_{S+G}, calculated as the sum of stellar mass M_S and gas mass M_G (Verheijen, 2001; Noordermeer and Verheijen, 2007; Zaritsky et al., 2014). This empirical relation is valid over several orders of magnitude and with an extremely small scatter. In the ΛCDM model, the rotation velocity should be primarily related to the total virial mass, represented mostly by the dark matter halo, $M \sim V^3$, but not to M_{S+G}. Since the dark matter halo is largely independent of baryonic processes, it is difficult to explain the observed extremely low scatter of the BTF relation (Lelli et al., 2016b; McGaugh et al., 2018; Lelli et al., 2019). If the most mass of a galaxy is formed by the baryonic dark matter located in the galaxy disk but not in the halo, the close relation between the stellar, gas and dust masses is expected.

4.2.3.4 Radial acceleration relation

A further close connection between mass of stars and gas M_{S+G} and the total mass M of galaxies, was revealed by McGaugh et al. (2016), when they studied a relation between the acceleration g_{S+G} due to mass M_{S+G} and the observed acceleration g_{obs} due to total mass M. The observed relation is fully empirical and points to a strong coupling between the mass of the dark matter and mass of stars and gas. Similarly as for the BTF relation, the observed coupling between g_{S+G} and g_{obs} is difficult to explain in the ΛCDM model.

4.2.3.5 Deficiency of Conformal Gravity and MOND theory

Although, the MOND theory matches some observations quite successfully, the theory was originally designed rather empirically to fit observations with no profound physical consistency. For example, some deep reasoning, why value of a_0 is within an order of magnitude of cH_0, is missing.

A common deficiency of MOND and CG seems violation of the GR equations. By contrast, theory presented in this paper explains satisfactorily the flat rotation curves and the above mentioned phenomena with no need to violate the GR theory. Nevertheless, we have to admit that the definitive resolution, whether GR or its modifications such as MOND (Milgrom, 1983a; Bekenstein, 2004; Milgrom, 2010; Milgrom, 2012) or Conformal Gravity (Mannheim, 2006; Mannheim and O'Brien, 2011; Mannheim and O'Brien, 2012; Mannheim, 2019) describe the gravitational field more appropriately, will need other future tests, e.g., based on detection of gravitational waves (Corda, 2009).

4.3 Morphology of spiral galaxies

Several theories have been proposed to explain the origin and evolution of structure of spiral galaxies and to predict basic properties of spiral arms (Toomre, 1977; Dobbs and Baba, 2014; Shu, 2016). Lindblad (1962) was the first, who assumed that the spiral structure arose from interaction between the orbits and gravitational forces of

the stars of the disk, and suggested to explain the spiral arms as density waves. This idea was further elaborated by Lin and Shu (1964) and Lin and Shu (1966) in their hypothesis of the quasi-stationary density waves, in which the spirals are formed by standing waves in the disk. They assume that the spiral pattern rotates in a particular angular frequency different from the rotation velocity of stars, which depends on the star distance from the galaxy centre. The formation of the global spiral pattern is considered as an instability of the stellar disk caused by the self-gravity. The density-wave theory was further developed and extended (Shu, 1970; Roberts et al., 1975; Sellwood and Carlberg, 1984; Elmegreen et al., 1999; Sellwood, 2011) and it is now the main tool for studying the gravitational stability of disk galaxies. The results are not decisive, but *N*-body simulations suggest that the spiral arms are transient and recurrent rather than quasi-stationary (Baba et al., 2009; Baba et al., 2013).

The density-wave theory faces, however, with several open questions and limitations. First, the theory is based on the classical Newtonian gravity, which neglects the space expansion. Second, predictions of the theory are uncertain. Still it is not clearly resolved, whether the spiral arms must be dynamic or whether the quasi-static arms are a feasible solution. Third, the observationally documented growth of the spiral galaxies with cosmic time is completely ignored and unexplained in this theory.

All the mentioned difficulties with modelling of spiral arms arise from the fact that the theory starts with rejecting an idea of spirals formed by stars and gas that remain fixed in the spirals. The reason is the so-called winding problem, when objects moving with the same orbital speed in the disk cause a differential rotation of material in galaxies (Ferreras, 2019). Since the length of orbits is shorter near the galaxy centre, the inner part of spirals winds up tighter than its outer part. Hence, a typical spiral pattern disappears after a few rotations. This idea is, however, simplistic and incorrect, because the GR effects in the galaxy evolution are ignored. If the space expansion and time dilation are considered, the galaxy size is growing and galaxy rotation speed varies with time. The spiral pattern is not destroyed, because it is continuously expanding. Consequently, the winding problem does not occur as demonstrated by numerical modelling in **Section 3**.

4.4 Solar system

Observations confirm that the global expansion affects also the solar system. Here we mention some of prominent examples (Anderson et al., 1998; Krizek, 2012; Iorio, 2015; Krizek et al., 2015; Krizek and Somer, 2015).

4.4.1 Faint young Sun paradox

According to the Standard solar model (Bahcall et al., 2001), the radius and luminosity of the Sun significantly evolved during the cosmic time. As the Sun is a star on the main sequence of the HR diagram, the solar radius was 4 Gyr ago about 89% of the solar radius at present and the luminosity was about 73.8% of the present luminosity (Bahcall et al., 2001, their tables 1 and 2). For a constant distance between the Sun and the Earth during this time span, such changes would have dramatic consequences for life conditions on the Earth (Ribas et al., 2010). The solar constant, i.e., the flux density at the Earth's mean orbital distance, is $I = 1.36\ \mathrm{kWm^{-2}}$ at present (Kopp and Lean, 2011), but 4 Gyr ago it was $I_0 = 1.00\ \mathrm{kWm^{-2}}$ only. Calculating the equilibrium temperature as

$$T^{\mathrm{eq}} = \left(\frac{I(1-A)}{4\sigma} \right)^{1/4}, \tag{35}$$

where $A = 0.3$ is the Earth's albedo (Goode et al., 2001) and σ is the Stefan-Boltzmann constant, we get $T^{\mathrm{eq}} = 254.5$ K and $T_0^{\mathrm{eq}} = 236.0$ K for the present time and for the past, respectively. Assuming the same level of the greenhouse effect (+32.5°C), the global average Earth's temperature would be −4.7°C in the past instead of 13.9°C observed at present (https://www.climate.gov/news-features/understanding-climate/climate-change-global-temperature). In fact, because of the ice albedo, the temperature would be even lower in the era of 4 Gyr ago. For the Earth's albedo of 0.5, we get $T_0^{\mathrm{eq}} = 249.4$ K and the global average Earth's temperature would be −23.8°C. By contrast, no glaciation is indicated from geological observations in the first 2.7 Gyr of the Earth's evolution (Bertotti et al., 2003) and water-related sediments have been found 3.8 Gyr ago (Windley, 1984). This severe discrepancy is known as the Faint young Sun paradox.

The paradox is resolved, if the expansion of the solar system is taken into account (Křížek, 2012; Křížek and Somer, 2015). The age of 4 Gyr corresponds to redshift $z = 0.46$ (see **Figure 1B**) and the orbital radius of the Earth was $(1+z)$ times shorter than at the present time. The flux corrected for a shorter orbital radius is easily calculated as $1.00 \times (1+z)^2 = 2.13\ \mathrm{kWm^{-2}}$ and the corresponding Earth's temperature is 44.5°C, provided we assume the same greenhouse effect as at present (+32.5°C). Hence, the temperature conditions on the Earth were convenient for life over the whole Earth's history. Note that higher temperatures of oceans (70°C) in the Precambrian era (3.5 Gyr ago) are independently indicated by observations of silicon and oxygen isotope data (Knauth, 2005; Robert and Chaussidon, 2006). The recession velocity of the Earth from the Sun comparable to the Hubble flow is indicated also from growth patterns on fossil corals observed for the time span of the last 500 Myr (Zhang et al., 2010).

4.4.2 Lunar orbit anomaly

The Moon's orbital distance is slowly increasing and the Earth's rotation rate is decreasing due to tidal forces transferring angular momentum from the Earth to the Moon. In order to investigate the Earth-Moon system, the Lunar Laser Ranging Experiment (LLR) from Apollo 11, 14, 15 and Lunokhod missions was performed to measure accurately the recession velocity of the Moon. The missions report the Moon's semimajor axis $d = 384,402$ km, which increases at rate (Dickey et al., 1994) of (3.82 ± 0.08) cm/yr. This value is anomalously high and inconsistent with an expected lunar recession velocity due to tidal forces, which should be lower by 30–45% (Křížek, 2009; Riofrio, 2012; Křížek and Somer, 2022). The observed lunar recession velocity would correspond to increasing Earth's rotation period at a rate of +2.3 ms per century, but only a rate of +1.8 ms per century is observed (Stephenson et al., 2016). In addition, numerical modelling of the orbital evolution under such tidal dissipation would imply the age of the lunar orbit to be 1.5×10^9 years, instead of 4×10^9 years suggested by observations (Bills and Ray, 1999). This discrepancy is known as the Lunar orbit anomaly and so far its origin is unclear.

If the expansion of the solar system is considered, the recession velocity of the Moon due to the expansion is 2.74 cm/yr assuming distance of the Moon $d = 384,402$ km and the Hubble

parameter $H_0 = 69.8\ \mathrm{kms}^{-1}\mathrm{Mpc}^{-1}$ (Freedman et al., 2019). Hence, the lunar recession velocity due to tides is reduced to 1.08 cm/yr that is more realistic. If the tides were fully responsible for the slowing Earth's rotation at rate of +1.8 ms per century, the lunar recession velocity would be ∼2.25 cm/yr. However, this is an upper limit only, because also other processes can slow down the Earth's rotation, such as impacts of massive meteorites, large earthquakes, huge volcanic eruptions, and energy dissipation in the Earth's mantle and the outer Earth's core due to convection.

4.4.3 Other observations

The Hubble flow in the solar system is indicated by many other observations (Křížek and Somer, 2015). Mars had to be much closer to the Sun in the past; it is dusty and icy at the present, but detailed images of the Martian surface reveal that it was formed by rivers in the period of 3–4 Gyr ago (Carr, 1995; Davis et al., 2016; Salese et al., 2020). Measurements of the Titan's orbital expansion rate by the Cassini spacecraft during ten close encounters of the Moon between 2006 and 2016 revealed that Titan rapidly migrates away from Saturn (Lainey et al., 2020). The Titan-Saturn mean distance is $d = 1,221,870$ km and the Titan's recession velocity is 11.3 cm/yr. The corresponding recession velocity due to the Hubble flow is 8.7 cm/yr. If this velocity is subtracted, the anomaly disappears and the resultant rate of 2.6 cm/yr produced by tidal forces becomes realistic. Also, the expansion of the solar system can explain the formation of Neptune and Kuiper belt, the existence of fast satellites of Mars, Jupiter, Uranus and Neptune that are below the stationary orbit, or the large orbital momentum of the Moon (Křížek and Somer, 2015).

5 Discussion and conclusion

The presented theory and numerical modelling satisfactorily explain several severe tensions between the standard ΛCDM model and observations.

- The improved Newtonian equations derived for the CC metric predict an increasing radius of gravitational orbits of local systems. The rate of growth with cosmic time is $(1+z)^{-1}$. This applies to all local systems including galaxy clusters, galaxies, and planetary systems. The gravitational orbits are stationary in the comoving coordinates but non-stationary in the proper coordinates.
- The existence of spirals in disk galaxies is a direct consequence of the space expansion and time dilation. The spirals are formed by the stellar mass and gas that remain fixed in them. The stellar mass and gas are continuously outflowed from the bulge-bar region into the spiral region. The spirals are detached from the bulge-bar region due to the space expansion.
- Since the orbital velocity of particles is conserved and the radius of orbits gradually increases during the space expansion, the spiral galaxies display flat rotation curves.

The constant rotation velocity, the space expansion and time dilation are the primary factors forming the morphology of spirals. The time dilation is particularly important, because a slower rate of time in the past significantly helped to separate spirals from the bulge-bar domain. As shown in the numerical modelling, the morphology of spirals depends on the expansion history of the Universe, on the galaxy mass, galaxy age and size of the bulge. Obviously, the presented modelling is rather simple and definitely far from being complete. A detailed parametric study based on observations of various types of galaxies is necessary for drawing more specific conclusions about the galaxy dynamics.

The previous theoretical attempts to correctly explain the galaxy dynamics were unsuccessful for the following reasons: 1) The simplest attempts ignored the space expansion and assumed galaxies in the static Universe. Consequently, the GR effects related to the expansion of the Universe were neglected and stars moved along stationary orbits not evolving in time. 2) Theories, which considered the space expansion using the GR theory, applied an incorrect cosmological model defined by the FLRW metric. This metric erroneously assumes that time is invariant of the space expansion. This assumption has fatal consequences for dynamics of local systems. An additional radial acceleration originating in the space expansion is included in the Newtonian equations for orbiting bodies, but the proper angular momentum $L = RV^{\phi}$ keeps constant. The constant L causes that the effect of the Hubble flow on the orbiting bodies is eliminated and the radius of the orbits is effectively insensitive to the space expansion.

By contrast, the proper angular momentum $L = RV^{\phi}$ in the Newtonian equations derived under the CC metric is not constant but it increases with redshift. Consequently, the orbits are not stationary any more, but their radius increases with cosmic time. Since the velocity of orbiting massive particles does not depend on the space expansion and the radius of orbits is continuously increasing, the rotation curves are essentially flat. Importantly, the rotation curves are flat without assuming non-baryonic dark matter haloes surrounding galaxies. No dark matter is needed for explaining all basic properties of the galactic dynamics. Applying the CC metric to interpretations of the SNe Ia dimming reveals that also dark energy is unnecessary for getting fit with observations (Behnke et al., 2002; Vavryčuk, 2022a). Hence, dark energy and dark matter are false and superfluous concepts originating in a wrong description of the space expansion, when the time dilation is ignored during the evolution of the Universe. Once a correct metric is applied, the cosmological model is consistent with observations with no need to introduce new unphysical concepts. A controversy of dark matter and dark energy concepts is evidenced also by many other observations (Kroupa, 2012; Weinberg et al., 2013; Kroupa, 2015; Buchert et al., 2016; Bull et al., 2016; Koyama, 2016; Bullock and Boylan-Kolchin, 2017; Ezquiaga and Zumalacárregui, 2017).

In addition, the presented theory resolves several other puzzles and paradoxes in cosmology. It explains the origin of spirals in a completely different way than proposed by the density-wave hypothesis. The spirals are not an effect of standing waves in the disk as so far believed (Toomre, 1977; Dobbs and Baba, 2014; Shu, 2016). Instead, they are objects formed by material remained fixed in spirals. Still, the winding problem is avoided. The theory also removes tensions related to the observed galaxy growth explained by major and/or minor mergers of galaxies. Since the hypothesis of mergers (Naab et al., 2009; Kormendy and Ho, 2013; McLure et al., 2013; Conselice, 2014) is refuted by observations of no evolution of the galaxy mass (Bundy et al., 2017; Kawinwanichakij et al., 2020), the problem of a galaxy growth is so far unsolved. The presented theory

also resolves challenges to the ΛCDM model such as the problem of faint satellite galaxies, the baryonic Tully-Fisher relation or the radial acceleration relation. Furthermore, numerous puzzles in the solar system are successfully explained such as the Faint young Sun paradox, the lunar orbit anomaly, the presence of rivers on ancient Mars, the Titan recession velocity anomaly, formation of the Kuiper belt and others (Dumin, 2015; Křížek et al., 2015; Křížek and Somer, 2015).

Data availability statement

The original contributions presented in the study are included in the article/supplementary material, further inquiries can be directed to the corresponding author.

Author contributions

VV is responsible for the whole study presented in the paper.

Funding

The Institute of Geophysics of the Czech Academy of Sciences supported this research.

Conflict of interest

The author declares that the research was conducted in the absence of any commercial or financial relationships that could be construed as a potential conflict of interest.

Publisher's note

References

Anderson, J. D., Laing, P. A., Lau, E. L., Liu, A. S., Nieto, M. M., and Turyshev, S. G. (1998). Indication, from Pioneer 10/11, Galileo, and Ulysses data, of an apparent anomalous, weak, long-range acceleration. *Phys. Rev. Lett.* 81, 2858–2861. doi:10.1103/PhysRevLett.81.2858

Baba, J., Asaki, Y., Makino, J., Miyoshi, M., Saitoh, T. R., and Wada, K. (2009). The origin of large peculiar motions of star-forming regions and spiral structures of our galaxy. *ApJ* 706, 471–481. doi:10.1088/0004-637X/706/1/471

Baba, J., Saitoh, T. R., and Wada, K. (2013). Dynamics of non-steady spiral arms in disk galaxies. *ApJ* 763, 46. doi:10.1088/0004-637X/763/1/46

Bahcall, J. N., Pinsonneault, M. H., and Basu, S. (2001). Solar models: Current epoch and time dependences, neutrinos, and helioseismological properties. *ApJ* 555, 990–1012. doi:10.1086/321493

Begeman, K. G., Broeils, A. H., and Sanders, R. H. (1991). Extended rotation curves of spiral galaxies: Dark haloes and modified dynamics. *MNRAS* 249, 523–537. doi:10.1093/mnras/249.3.523

Begeman, K. G. (1987). *HI rotation curves of spiral galaxies*. Ph.D. thesis. Groningen: University of Groningen, Kapteyn Astronomical Institute.

Begeman, K. G. (1989). HI rotation curves of spiral galaxies. I. NGC 3198. *Astron. Astrophys.* 223, 47–60.

Behnke, D., Blaschke, D. B., Pervushin, V. N., and Proskurin, D. (2002). Description of supernova data in conformal cosmology without cosmological constant. *Phys. Lett. B* 530, 20–26. doi:10.1016/S0370-2693(02)01341-2

Bekenstein, J. D. (2004). Relativistic gravitation theory for the modified Newtonian dynamics paradigm. *Phys. Rev. D.* 70, 083509. doi:10.1103/PhysRevD.70.083509

Bergström, L. (2000). Non-baryonic dark matter: Observational evidence and detection methods. *Rep. Prog. Phys.* 63, 793–841. doi:10.1088/0034-4885/63/5/2r3

Bertone, G., and Hooper, D. (2018). History of dark matter. *Rev. Mod. Phys.* 90, 045002. doi:10.1103/RevModPhys.90.045002

Bertotti, B., Farinella, P., and Vokrouhlick, D. (2003). Physics of the solar system - dynamics and evolution, space physics, and spacetime structure. *Astrophysics and Space Science Library*.293. doi:10.1007/978-94-010-0233-2

Bills, B. G., and Ray, R. D. (1999). Lunar orbital evolution: A synthesis of recent results. *Geophys. Res. Lett.* 26, 3045–3048. doi:10.1029/1999GL008348

Binney, J., Gerhard, O., and Spergel, D. (1997). The photometric structure of the inner Galaxy. *MNRAS* 288, 365–374. doi:10.1093/mnras/288.2.365

Bissantz, N., and Gerhard, O. (2002). Spiral arms, bar shape and bulge microlensing in the Milky Way. *MNRAS* 330, 591–608. doi:10.1046/j.1365-8711.2002.05116.x

Bolen, B., Bombelli, L., and Puzio, R. (2001). Expansion-induced contribution to the precession of binary orbits. *Class. Quantum Gravity* 18, 1173–1178. doi:10.1088/0264-9381/18/7/302

Bournaud, F., Jog, C. J., and Combes, F. (2007). Multiple minor mergers: Formation of elliptical galaxies and constraints for the growth of spiral disks. *Astron. Astrophys.* 476, 1179–1190. doi:10.1051/0004-6361:20078010

Bouwens, R. J., Illingworth, G. D., Blakeslee, J. P., Broadhurst, T. J., and Franx, M. (2004). Galaxy size evolution at high redshift and surface brightness selection effects: Constraints from the Hubble ultra deep field. *ApJ* 611, L1–L4. doi:10.1086/423786

Buchert, T., Coley, A. A., Kleinert, H., Roukema, B. F., and Wiltshire, D. L. (2016). Observational challenges for the standard FLRW model. *Int. J. Mod. Phys. D* 25, 1630007–1630244. doi:10.1142/S021827181630007X

Bugg, D. V. (2015). Mond — a review. *Can. J. Phys.* 93, 119–125. doi:10.1139/cjp-2014-0057

Bull, P., Akrami, Y., Adamek, J., Baker, T., Bellini, E., Beltrán Jiménez, J., et al. (2016). Beyond ΛCDM: Problems, solutions, and the road ahead. *Phys. Dark Universe* 12, 56–99. doi:10.1016/j.dark.2016.02.001

Bullock, J. S., and Boylan-Kolchin, M. (2017). Small-scale challenges to the ΛCDM paradigm. *Annu. Rev. Astronomy Astrophysics* 55, 343–387. doi:10.1146/annurev-astro-091916-055313

Bundy, K., Leauthaud, A., Saito, S., Maraston, C., Wake, D. A., and Thomas, D. (2017). The Stripe 82 Massive Galaxy Project. III. A lack of growth among massive galaxies. *ApJ* 851, 34. doi:10.3847/1538-4357/aa9896

Callan, C., Dicke, R. H., and Peebles, P. J. E. (1965). Cosmology and Newtonian mechanics. *Am. J. Phys.* 33, 105–108. doi:10.1119/1.1971256

Calzetti, D., Armus, L., Bohlin, R. C., Kinney, A. L., Koornneef, J., and Storchi-Bergmann, T. (2000). The dust content and opacity of actively star-forming galaxies. *ApJ* 533, 682–695. doi:10.1086/308692

Carr, M. H. (1995). The Martian drainage system and the origin of valley networks and fretted channels. *J. Geophys. Res.* 100, 7479–7508. doi:10.1029/95JE00260

Carrera, M., and Giulini, D. (2010). Influence of global cosmological expansion on local dynamics and kinematics. *Rev. Mod. Phys.* 82, 169–208. doi:10.1103/RevModPhys.82.169

Conselice, C. J. (2014). The evolution of galaxy structure over cosmic time. *Annu. Rev. Astron. Astrophys.* 52, 291–337. doi:10.1146/annurev-astro-081913-040037

Cooperstock, F. I., Faraoni, V., and Vollick, D. N. (1998). The influence of the cosmological expansion on local systems. *ApJ* 503, 61–66. doi:10.1086/305956

Corda, C. (2009). Interferometric detection of gravitational waves: The definitive test for General Relativity. *Int. J. Mod. Phys. D* 18, 2275–2282. doi:10.1142/S0218271809015904

da Cunha, E., Charlot, S., and Elbaz, D. (2008). A simple model to interpret the ultraviolet, optical and infrared emission from galaxies. *MNRAS* 388, 1595–1617. doi:10.1111/j.1365-2966.2008.13535.x

Dabrowski, M. P., Garecki, J., and Blaschke, D. B. (2009). Conformal transformations and conformal invariance in gravitation. *Ann. Phys.* 521, 13–32. doi:10.1002/andp.20095210105

Dahlen, T., Mobasher, B., Dickinson, M., Ferguson, H. C., Giavalisco, M., Kretchmer, C., et al. (2007). Evolution of the luminosity function, star formation rate, morphology, and size of star-forming galaxies selected at rest-frame 1500 and 2800 Å. *ApJ* 654, 172–185. doi:10.1086/508854

Davis, J., Balme, M., Grindrod, P., Williams, R., and Gupta, S. (2016). Extensive Noachian fluvial systems in Arabia Terra: Implications for early Martian climate. *Geology* 44, 847–850. doi:10.1130/G38247.1

Davis, M., Efstathiou, G., Frenk, C. S., and White, S. D. M. (1985). The evolution of large-scale structure in a universe dominated by cold dark matter. *ApJ* 292, 371–394. doi:10.1086/163168

de Blok, W. J. G., Walter, F., Brinks, E., Trachternach, C., Oh, S. H., and Kennicutt, J. R. C. (2008). High-resolution rotation curves and galaxy mass models from THINGS. *AJ* 136, 2648–2719. doi:10.1088/0004-6256/136/6/2648

de Blok, W. J. G., and Bosma, A. (2002). High-resolution rotation curves of low surface brightness galaxies. *Astron. Astrophys.* 385, 816–846. doi:10.1051/0004-6361:20020080

de Blok, W. J. G., McGaugh, S. S., and Rubin, V. C. (2001). High-resolution rotation curves of low surface brightness galaxies. II. Mass models. *AJ* 122, 2396–2427. doi:10.1086/323450

Del Popolo, A., and Le Delliou, M. (2017). Small scale problems of the ΛCDM model: A short review. *Galaxies* 5, 17. doi:10.3390/galaxies5010017

Dicke, R. H., and Peebles, P. J. (1964). Evolution of the solar system and the expansion of the universe. *Phys. Rev. Lett.* 12, 435–437. doi:10.1103/PhysRevLett.12.435

Dickey, J. O., Bender, P. L., Faller, J. E., Newhall, X. X., Ricklefs, R. L., Ries, J. G., et al. (1994). Lunar laser ranging: A continuing legacy of the Apollo program. *Science* 265, 482–490. doi:10.1126/science.265.5171.482

Dobbs, C., and Baba, J. (2014). Dawes review 4: Spiral structures in disc galaxies. *Publ. Astron. Soc. Aust.*, 31, e035. doi:10.1017/pasa.2014.31

Draine, B. T., and Li, A. (2007). Infrared emission from interstellar dust. IV. The silicate-graphite-PAH model in the Post-Spitzer era. *ApJ* 657, 810–837. doi:10.1086/511055

Dubinski, J., and Carlberg, R. G. (1991). The structure of cold dark matter halos. *ApJ* 378, 496. doi:10.1086/170451

Duc, P. A., Paudel, S., McDermid, R. M., Cuillandre, J. C., Serra, P., Bournaud, F., et al. (2014). Identification of old tidal dwarfs near early-type galaxies from deep imaging and H I observations. *MNRAS* 440, 1458–1469. doi:10.1093/mnras/stu330

Dumin, Y. V. (2015). The faint young Sun paradox in the context of modern cosmology. *Astron. Tsirkulyar* 1623, 1–5.

Dunne, L., Eales, S., Edmunds, M., Ivison, R., Alexander, P., and Clements, D. L. (2000). The SCUBA Local Universe Galaxy Survey - I. First measurements of the submillimetre luminosity and dust mass functions. *MNRAS* 315, 115–139. doi:10.1046/j.1365-8711.2000.03386.x

Einstein, A. (1920). "Relativity, the special and the general theory," in *Authorized translation by*. Editor W. L. Robert (Henry Holt and Company), 168.

Einstein, A., and Straus, E. G. (1945). The influence of the expansion of space on the gravitation fields surrounding the individual stars. *Rev. Mod. Phys.* 17, 120–124. doi:10.1103/RevModPhys.17.120

Elmegreen, D. M., Chromey, F. R., Bissell, B. A., and Corrado, K. (1999). K'-Band observations of underlying symmetric structure in flocculent galaxies. *AJ* 118, 2618–2624. doi:10.1086/301127

Endean, G. (1997). Cosmology in conformally flat spacetime. *ApJ* 479, 40–45. doi:10.1086/303862

Endean, G. (1994). Redshift and the Hubble constant in conformally flat spacetime. *ApJ* 434, 397. doi:10.1086/174741

Ezquiaga, J. M., and Zumalacárregui, M. (2017). Dark energy after GW170817: Dead ends and the road ahead. *Phys. Rev. Lett.* 119, 251304. doi:10.1103/PhysRevLett.119.251304

Faraoni, V., and Jacques, A. (2007). Cosmological expansion and local physics. *Phys. Rev. D.* 76, 063510. doi:10.1103/PhysRevD.76.063510

Ferreras, I. (2019). *Fundamentals of galaxy dynamics*. London: Formation and Evolution (UCL Press).

Freedman, W. L., Madore, B. F., Gibson, B. K., Ferrarese, L., Kelson, D. D., Sakai, S., et al. (2001). Final results from the Hubble space telescope key project to measure the Hubble constant. *ApJ* 553, 47–72. doi:10.1086/320638

Freedman, W. L., Madore, B. F., Hatt, D., Hoyt, T. J., Jang, I. S., Beaton, R. L., et al. (2019). The Carnegie-Chicago Hubble program. VIII. An independent determination of the Hubble constant based on the tip of the red giant branch. *ApJ* 882, 34. doi:10.3847/1538-4357/ab2f73

Friedmann, A. (1922). Über die Krümmung des Raumes. *Z. für Phys.* 10, 377–386. doi:10.1007/BF01332580

Galianni, P., Patat, F., Higdon, J. L., Mieske, S., and Kroupa, P. (2010). VLT observations of NGC 1097's "dog-leg" tidal stream. Dwarf spheroidals and tidal streams. *Astron. Astrophys.* 521, A20. doi:10.1051/0004-6361/200913518

Goldhaber, G., Deustua, S., Gabi, S., Groom, D., Hook, I., Kim, A., et al. (1997). "Observation of cosmological time dilation using Type Ia supernovae as clocks," in *Thermonuclear supernovae*. Editors P. Ruiz-Lapuente, R. Canal, and J. Isern (Dordrecht: Springer), 486, 777. doi:10.1007/978-94-011-5710-0_48

Goldhaber, G., Groom, D. E., Kim, A., Aldering, G., Astier, P., Conley, A., et al. (2001). Timescale stretch parameterization of type Ia supernova B-band light curves. *ApJ* 558, 359–368. doi:10.1086/322460

Goobar, A., and Leibundgut, B. (2011). Supernova cosmology: Legacy and future. *Annu. Rev. Nucl. Part. Sci.* 61, 251–279. doi:10.1146/annurev-nucl-102010-130434

Goode, P. R., Qiu, J., Yurchyshyn, V., Hickey, J., Chu, M. C., Kolbe, E., et al. (2001). Earthshine observations of the Earth's reflectance. *Geophys. Res. Lett.* 28, 1671–1674. doi:10.1029/2000GL012580

Grøn, Ø., and Johannesen, S. (2011). FRW universe models in conformally flat-spacetime coordinates I: General formalism. *Eur. Phys. J. Plus* 126, 28. doi:10.1140/epjp/i2011-11028-6

Harada, T., Carr, B. J., and Igata, T. (2018). Complete conformal classification of the Friedmann-Lemaître-Robertson-Walker solutions with a linear equation of state. *Class. Quantum Gravity* 35, 105011. doi:10.1088/1361-6382/aab99f

Holwerda, B. W., Bouwens, R., Oesch, P., Smit, R., Illingworth, G., and Labbe, I. (2015). The sizes of candidate galaxies$z\sim$ 9–10: confirmation of the bright CANDELS sample and relation with luminosity and mass. *ApJ* 808, 6. doi:10.1088/0004-637X/808/1/6

Hubble, E. (1929). A relation between distance and radial velocity among extra-galactic nebulae. *Proc. Natl. Acad. Sci.* 15, 168–173. doi:10.1073/pnas.15.3.168

Ibison, M. (2007). On the conformal forms of the Robertson-Walker metric. *J. Math. Phys.* 48, 122501. doi:10.1063/1.2815811

Infeld, L., and Schild, A. (1945). A new approach to kinematic cosmology. *Phys. Rev.* 68, 250–272. doi:10.1103/PhysRev.68.250

Infeld, L., and Schild, A. E. (1946). A new approach to kinematic cosmology-(B). *Phys. Rev.* 70, 410–425. doi:10.1103/PhysRev.70.410

Iorio, L. (2015). Gravitational anomalies in the solar system? *Int. J. Mod. Phys. D* 24, 1530015–1530343. doi:10.1142/S0218271815300153

Iorio, L. (2013). Local cosmological effects of the order of H in the orbital motion of a binary system. *MNRAS* 429, 915–922. doi:10.1093/mnras/sts396

Jacoby, G. H., Branch, D., Ciardullo, R., Davies, R. L., Harris, W. E., Pierce, M. J., et al. (1992). A critical review of selected techniques for measuring extragalactic distances. *PASP* 104, 599. doi:10.1086/133035

Kastrup, H. A. (2008). On the advancements of conformal transformations and their associated symmetries in geometry and theoretical physics. *Ann. Phys.* 520, 631–690. doi:10.1002/andp.200852009-1005

Kauffmann, G., White, S. D. M., and Guiderdoni, B. (1993). The formation and evolution of galaxies within merging dark matter haloes. *MNRAS* 264, 201–218. doi:10.1093/mnras/264.1.201

Kawinwanichakij, L., Papovich, C., Ciardullo, R., Finkelstein, S. L., Stevans, M. L., Wold, I. G. B., et al. (2020). On the (lack of) evolution of the stellar mass function of massive galaxies from z = 1.5 to 0.4. *ApJ* 892, 7. doi:10.3847/1538-4357/ab75c4

Knauth, L. P. (2005). Temperature and salinity history of the precambrian ocean: Implications for the course of microbial evolution. *Palaeogeogr. Palaeoclimatol. Palaeoecol.* 219, 53–69. doi:10.1016/j.palaeo.2004.10.014

Kopp, G., and Lean, J. L. (2011). A new, lower value of total solar irradiance: Evidence and climate significance. *Geophys. Res. Lett.* 38, L01706. doi:10.1029/2010GL045777

Kormendy, J., and Ho, L. C. (2013). Coevolution (or not) of supermassive black holes and host galaxies. *Annu. Rev. Astron. Astrophys.* 51, 511–653. doi:10.1146/annurev-astro-082708-101811

Koyama, K. (2016). Cosmological tests of modified gravity. *Rep. Prog. Phys.* 79, 046902. doi:10.1088/0034-4885/79/4/046902

Křížek, M. (2012). Dark energy and the anthropic principle. *New Astron.* 17, 1–7. doi:10.1016/j.newast.2011.05.003

Křížek, M. (2009). Does a gravitational aberration contribute to the accelerated expansion of the universe? *Commun. Comput. Phys.* 5, 1030–1044.

Křížek, M., Křížek, F., and Somer, L. (2015). *Antigravity - its origin and manifestations*. Saarbruecken: Lambert Academic Publishing.

Křížek, M., and Somer, L. (2022). Anthropic principle and the Hubble-Lemaître constant. *Galaxies* 10, 71. doi:10.3390/galaxies10030071

Křížek, M., and Somer, L. (2015). Manifestations of dark energy in the solar system. *Gravit. Cosmol.* 21, 59–72. doi:10.1134/S0202289315010090

Kroupa, P., Famaey, B., de Boer, K. S., Dabringhausen, J., Pawlowski, M. S., Boily, C. M., et al. (2010). Local-Group tests of dark-matter concordance cosmology. Towards a new paradigm for structure formation. *Astron. Astrophys.* 523, A32. doi:10.1051/0004-6361/201014892

Kroupa, P. (2015). Galaxies as simple dynamical systems: Observational data disfavor dark matter and stochastic star formation. *Can. J. Phys.* 93, 169–202. doi:10.1139/cjp-2014-0179

Kroupa, P. (2012). The dark matter crisis: Falsification of the current standard model of cosmology. *Publ. Astron. Soc. Aust.*, 29, 395–433. doi:10.1071/AS12005

Lainey, V., Casajus, L. G., Fuller, J., Zannoni, M., Tortora, P., Cooper, N., et al. (2020). Resonance locking in giant planets indicated by the rapid orbital expansion of Titan. *Nat. Astron.* 4, 1053–1058. doi:10.1038/s41550-020-1120-5

Leibundgut, B. (2001). Cosmological implications from observations of type Ia supernovae. *Annu. Rev. Astron. Astrophys.* 39, 67–98. doi:10.1146/annurev.astro.39.1.67

Leibundgut, B., Schommer, R., Phillips, M., Riess, A., Schmidt, B., Spyromilio, J., et al. (1996). Time dilation in the light curve of the distant type IA supernova SN 1995K. *ApJ* 466, L21–L24. doi:10.1086/310164

Lelli, F., McGaugh, S. S., Schombert, J. M., Desmond, H., and Katz, H. (2019). The baryonic Tully-Fisher relation for different velocity definitions and implications for galaxy angular momentum. *MNRAS* 484, 3267–3278. doi:10.1093/mnras/stz205

Lelli, F., McGaugh, S. S., and Schombert, J. M. (2016). Sparc: Mass models for 175 disk galaxies with Spitzer photometry and accurate rotation curves. *AJ* 152, 157. doi:10.3847/0004-6256/152/6/157

Lelli, F., McGaugh, S. S., and Schombert, J. M. (2016). The small scatter of the baryonic Tully-Fisher relation. *ApJ* 816, L14. doi:10.3847/2041-8205/816/1/L14

Lemaître, G. (1927). Un Univers homogène de masse constante et de rayon croissant rendant compte de la vitesse radiale des nébuleuses extra-galactiques. *Ann. Société Sci. Brux.* 47, 49–59.

Lerner, E. J. (2018). Observations contradict galaxy size and surface brightness predictions that are based on the expanding universe hypothesis. *MNRAS* 477, 3185–3196. doi:10.1093/mnras/sty728

Lin, C. C., and Shu, F. H. (1964). On the spiral structure of disk galaxies. *ApJ* 140, 646. doi:10.1086/147955

Lin, C. C., and Shu, F. H. (1966). On the spiral structure of disk galaxies, II. Outline of a theory of density waves. *Proc. Natl. Acad. Sci.* 55, 229–234. doi:10.1073/pnas.55.2.229

Lindblad, B. (1962). "Theories of spiral structure in galaxies," in *Problems of extra-galactic research*. Editor G. C. McVittie, 15, 146.

Maddox, S. J., Efstathiou, G., Sutherland, W. J., and Loveday, J. (1990). Galaxy correlations on large scales. *MNRAS* 242, 43P–47P. doi:10.1093/mnras/242.1.43P

Man, A. W. S., Toft, S., Zirm, A. W., Wuyts, S., and van der Wel, A. (2012). The pair fraction of massive galaxies at $0 \leqslant z \leqslant 3$. *ApJ* 744, 85. doi:10.1088/0004-637X/744/2/85

Man, A. W. S., Zirm, A. W., and Toft, S. (2016). Resolving the discrepancy of galaxy merger fraction measurements at $z \sim 0$-3. *ApJ* 830, 89. doi:10.3847/0004-637X/830/2/89

Mannheim, P. D. (2006). Alternatives to dark matter and dark energy. *Prog. Part. Nucl. Phys.* 56, 340–445. doi:10.1016/j.ppnp.2005.08.001

Mannheim, P. D. (1990). Conformal cosmology with no cosmological constant. *General Relativ. Gravit.* 22, 289–298. doi:10.1007/BF00756278

Mannheim, P. D. (2019). Is dark matter fact or fantasy? — clues from the data. *Int. J. Mod. Phys. D* 28, 1944022. doi:10.1142/S021827181944022X

Mannheim, P. D. (2012). Making the case for conformal gravity. *Found. Phys.* 42, 388–420. doi:10.1007/s10701-011-9608-6

Mannheim, P. D., and O'Brien, J. G. (2012). Fitting galactic rotation curves with conformal gravity and a global quadratic potential. *Phys. Rev. D.* 85, 124020. doi:10.1103/PhysRevD.85.124020

Mannheim, P. D., and O'Brien, J. G. (2011). Impact of a global quadratic potential on galactic rotation curves. *Phys. Rev. Lett.* 106, 121101. doi:10.1103/PhysRevLett.106.121101

Mathewson, D. S., Ford, V. L., and Buchhorn, M. (1992). A southern sky survey of the peculiar velocities of 1355 spiral galaxies. *ApJS* 81, 413. doi:10.1086/191700

McGaugh, S. S., Lelli, F., and Schombert, J. M. (2016). Radial acceleration relation in rotationally supported galaxies. *Phys. Rev. Lett.* 117, 201101. doi:10.1103/PhysRevLett.117.201101

McGaugh, S. S., Li, P., Lelli, F., and Schombert, J. M. (2018). Presence of a fundamental acceleration scale in galaxies. *Nat. Astron.* 2, 924. doi:10.1038/s41550-018-0615-9

McGaugh, S. S. (2019). The imprint of spiral arms on the galactic rotation curve. *ApJ* 885, 87. doi:10.3847/1538-4357/ab479b

McGaugh, S. S. (2016). The surface density profile of the galactic disk from the terminal velocity curve. *ApJ* 816, 42. doi:10.3847/0004-637X/816/1/42

McLure, R. J., Pearce, H. J., Dunlop, J. S., Cirasuolo, M., Curtis-Lake, E., Bruce, V. A., et al. (2013). The sizes, masses and specific star formation rates of massive galaxies at $1.3 < z < 1.5$: Strong evidence in favour of evolution via minor mergers. *MNRAS* 428, 1088–1106. doi:10.1093/mnras/sts092

McVittie, G. C. (1933). The mass-particle in an expanding universe. *MNRAS* 93, 325–339. doi:10.1093/mnras/93.5.325

Milgrom, M. (1983). A modification of the Newtonian dynamics - implications for galaxies. *ApJ* 270, 371–383. doi:10.1086/161131

Milgrom, M. (1983). A modification of the Newtonian dynamics as a possible alternative to the hidden mass hypothesis. *ApJ* 270, 365–370. doi:10.1086/161130

Milgrom, M. (2010). Quasi-linear formulation of MOND. *MNRAS* 403, 886–895. doi:10.1111/j.1365-2966.2009.16184.x

Milgrom, M. (2012). Testing MOND over a wide acceleration range in X-ray ellipticals. *Phys. Rev. Lett.* 109, 131101. doi:10.1103/PhysRevLett.109.131101

Mo, H. J., Mao, S., and White, S. D. M. (1998). The formation of galactic discs. *MNRAS* 295, 319–336. doi:10.1046/j.1365-8711.1998.01227.x

Moore, B., Ghigna, S., Governato, F., Lake, G., Quinn, T., Stadel, J., et al. (1999). Dark matter substructure within galactic halos. *ApJ* 524, L19–L22. doi:10.1086/312287

Mould, J. R., Huchra, J. P., Freedman, W. L., Kennicutt J Robert, C., Ferrarese, L., Ford, H. C., et al. (2000). The Hubble Space Telescope Key Project on the extragalactic distance scale. XXVIII. Combining the constraints on the Hubble constant. *ApJ* 529, 786–794. doi:10.1086/308304

Mundy, C. J., Conselice, C. J., Duncan, K. J., Almaini, O., Häußler, B., and Hartley, W. G. (2017). A consistent measure of the merger histories of massive galaxies using close-pair statistics - I. Major mergers at $z < 3.5$. *MNRAS* 470, 3507–3531. doi:10.1093/mnras/stx1238

Naab, T., Johansson, P. H., and Ostriker, J. P. (2009). Minor mergers and the size evolution of elliptical galaxies. *ApJ* 699, L178–L182. doi:10.1088/0004-637X/699/2/L178

Nandra, R., Lasenby, A. N., and Hobson, M. P. (2012). The effect of a massive object on an expanding universe. *MNRAS* 422, 2931–2944. doi:10.1111/j.1365-2966.2012.20618.x

Navarro, J. F., Frenk, C. S., and White, S. D. M. (1997). A universal density profile from hierarchical clustering. *ApJ* 490, 493–508. doi:10.1086/304888

Navarro, J. F., Frenk, C. S., and White, S. D. M. (1996). The structure of cold dark matter halos. *ApJ* 462, 563. doi:10.1086/177173

Newman, A. B., Ellis, R. S., Bundy, K., and Treu, T. (2012). Can minor merging account for the size growth of quiescent galaxies? New results from the CANDELS survey. *ApJ* 746, 162. doi:10.1088/0004-637X/746/2/162

Noerdlinger, P. D., and Petrosian, V. (1971). The effect of cosmological expansion on self-gravitating ensembles of particles. *ApJ* 168, 1. doi:10.1086/151054

Noordermeer, E., and Verheijen, M. A. W. (2007). The high-mass end of the Tully-Fisher relation. *MNRAS* 381, 1463–1472. doi:10.1111/j.1365-2966.2007.12369.x

O'Brien, J. G., and Mannheim, P. D. (2012). Fitting dwarf galaxy rotation curves with conformal gravity. *MNRAS* 421, 1273–1282. doi:10.1111/j.1365-2966.2011.20386.x

Oesch, P. A., Bouwens, R. J., Carollo, C. M., Illingworth, G. D., Trenti, M., Stiavelli, M., et al. (2010). Structure and morphologies of $z \sim 7$-8 galaxies from ultra-deep WFC3/IR imaging of the Hubble Ultra-Deep Field. *ApJ* 709, L21–L25. doi:10.1088/2041-8205/709/1/L21

Pachner, J. (1964). Nonconservation of energy during cosmic evolution. *Phys. Rev. Lett.* 12, 117–118. doi:10.1103/PhysRevLett.12.117

Pawlowski, M. S., and Kroupa, P. (2013). The rotationally stabilized VPOS and predicted proper motions of the Milky Way satellite galaxies. *MNRAS* 435, 2116–2131. doi:10.1093/mnras/stt1429

Pawlowski, M. S., and McGaugh, S. S. (2014). Perseus I and the NGC 3109 association in the context of the Local Group dwarf galaxy structures. *MNRAS* 440, 908–919. doi:10.1093/mnras/stu321

Peacock, J. A. (1999). *Cosmological physics*. Cambridge: Cambridge University Press.

Persic, M., Salucci, P., and Stel, F. (1996). The universal rotation curve of spiral galaxies — I. The dark matter connection. *MNRAS* 281, 27–47. doi:10.1093/mnras/278.1.27

Phillips, M. M., Lira, P., Suntzeff, N. B., Schommer, R. A., Hamuy, M., and Maza, J. (1999). The reddening-free decline rate versus luminosity relationship for type Ia supernovae. *AJ* 118, 1766–1776. doi:10.1086/301032

Phillips, M. M. (1993). The absolute magnitudes of type IA supernovae. *ApJ* 413, L105. doi:10.1086/186970

Ribas, I. (2010). "The Sun and stars as the primary energy input in planetary atmospheres," in *Solar and stellar variability: Impact on Earth and planets*. Editors A. G. Kosovichev, A. H. Andrei, and J. P. Rozelot, 264, 3–18. doi:10.1017/S1743921309992298

Riofrio, L. (2012). Calculation of lunar orbit anomaly. *Planet. Sci.* 1, 1. doi:10.1186/2191-2521-1-1

Robert, F., and Chaussidon, M. (2006). A palaeotemperature curve for the Precambrian oceans based on silicon isotopes in cherts. *Nature* 443, 969–972. doi:10.1038/nature05239

Roberts, J. W. W., Roberts, M. S., and Shu, F. H. (1975). Density wave theory and the classification of spiral galaxies. *ApJ* 196, 381–405. doi:10.1086/153421

Rubin, V. C., Burstein, D., Ford, J. W. K., and Thonnard, N. (1985). Rotation velocities of 16 SA galaxies and a comparison of Sa, SB and SC rotation properties. *ApJ* 289, 81–104. doi:10.1086/162866

Rubin, V. C., Ford, J. W. K., and Thonnard, N. (1980). Rotational properties of 21 SC galaxies with a large range of luminosities and radii, from NGC 4605 (R=4 kpc) to UGC 2885 (R=122 kpc). *ApJ* 238, 471–487. doi:10.1086/158003

Rubin, V. C., and Ford, W. K. (1970). Rotation of the Andromeda nebula from a spectroscopic survey of emission regions. *ApJ* 159, 379. doi:10.1086/150317

Ryden, B. (2016). *Introduction to cosmology*. Cambridge: Cambridge University Press.

Salese, F., McMahon, W. J., Balme, M. R., Ansan, V., Davis, J. M., and Kleinhans, M. G. (2020). Sustained fluvial deposition recorded in Mars' Noachian stratigraphic record. *Nat. Commun.* 11, 2067. doi:10.1038/s41467-020-15622-0

Sanders, R. H., and McGaugh, S. S. (2002). Modified Newtonian dynamics as an alternative to dark matter. *Annu. Rev. Astron. Astrophys.* 40, 263–317. doi:10.1146/annurev.astro.40.060401.093923

Sanders, R. H. (1996). The published extended rotation curves of spiral galaxies: Confrontation with modified dynamics. *ApJ* 473, 117–129. doi:10.1086/178131

Sandstrom, K. M., Leroy, A. K., Walter, F., Bolatto, A. D., Croxall, K. V., Draine, B. T., et al. (2013). The CO-to-H_2 conversion factor and dust-to-gas ratio on kiloparsec scales in nearby galaxies. *ApJ* 777, 5. doi:10.1088/0004-637X/777/1/5

Schneider, P. (2015). *Extragalactic Astronomy and cosmology: An introduction*. New York: Springer. doi:10.1007/978-3-642-54083-7

Sellwood, J. A., and Carlberg, R. G. (1984). Spiral instabilities provoked by accretion and star formation. *ApJ* 282, 61–74. doi:10.1086/162176

Sellwood, J. A. (2011). The lifetimes of spiral patterns in disc galaxies. *MNRAS* 410, 1637–1646. doi:10.1111/j.1365-2966.2010.17545.x

Sereno, M., and Jetzer, P. (2007). Evolution of gravitational orbits in the expanding universe. *Phys. Rev. D.* 75, 064031. doi:10.1103/PhysRevD.75.064031

Shibuya, T., Ouchi, M., and Harikane, Y. (2015). Morphologies of ∼190,000 galaxies at z = 0-10 revealed with HST legacy data. I. Size evolution. *ApJS* 219, 15. doi:10.1088/0067-0049/219/2/15

Shu, F. H. (1970). On the density-wave theory of galactic spirals. I. Spiral structure as a normal mode of oscillation. *ApJ* 160, 89. doi:10.1086/150409

Shu, F. H. (2016). Six decades of spiral density wave theory. *Annu. Rev. Astron. Astrophys.*, 54, 667–724. doi:10.1146/annurev-astro-081915-023426

Sofue, Y. (2017). Rotation and mass in the Milky Way and spiral galaxies. *PASJ* 69, R1. doi:10.1093/pasj/psw103

Sofue, Y. (2016). Rotation curve decomposition for size-mass relations of bulge, disk, and dark halo components in spiral galaxies. *PASJ* 68, 2. doi:10.1093/pasj/psv103

Sofue, Y., and Rubin, V. (2001). Rotation curves of spiral galaxies. *Annu. Rev. Astron. Astrophys.* 39, 137–174. doi:10.1146/annurev.astro.39.1.137

Stephenson, F. R., Morrison, L. V., and Hohenkerk, C. Y. (2016). Measurement of the Earth's rotation: 720 BC to AD 2015. *Proc. R. Soc. Lond. Ser. A* 472, 20160404. doi:10.1098/rspa.2016.0404

Swaters, R. A., Madore, B. F., and Trewhella, M. (2000). High-resolution rotation curves of low surface brightness galaxies. *ApJ* 531, L107–L110. doi:10.1086/312540

Swaters, R. A., Madore, B. F., van den Bosch, F. C., and Balcells, M. (2003). The central mass distribution in dwarf and low surface brightness galaxies. *ApJ* 583, 732–751. doi:10.1086/345426

Taylor, E. N., Franx, M., Glazebrook, K., Brinchmann, J., van der Wel, A., and van Dokkum, P. G. (2010). On the dearth of compact, massive, red sequence galaxies in the local universe. *ApJ* 720, 723–741. doi:10.1088/0004-637X/720/1/723

Tiley, A. L., Swinbank, A. M., Harrison, C. M., Smail, I., Turner, O. J., Schaller, M., et al. (2019). The shapes of the rotation curves of star-forming galaxies over the last ≈ 10 Gyr. *MNRAS* 485, 934–960. doi:10.1093/mnras/stz428

Toomre, A. (1977). Theories of spiral structure. *Annu. Rev. Astron. Astrophys.* 15, 437–478. doi:10.1146/annurev.aa.15.090177.002253

Trujillo, I., Förster Schreiber, N. M., Rudnick, G., Barden, M., Franx, M., Rix, H. W., et al. (2006). The size evolution of galaxies since z∼3: Combining SDSS, GEMS, and FIRES. *ApJ* 650, 18–41. doi:10.1086/506464

Tully, R. B., and Fisher, J. R. (1977). A new method of determining distances to galaxies. *Astron. Astrophys.* 54, 661–673.

van Albada, T. S., Bahcall, J. N., Begeman, K., and Sancisi, R. (1985). Distribution of dark matter in the spiral galaxy NGC 3198. *ApJ* 295, 305–313. doi:10.1086/163375

van der Wel, A., Franx, M., van Dokkum, P. G., Skelton, R. E., Momcheva, I. G., Whitaker, K. E., et al. (2014). 3D-HST+CANDELS: The evolution of the galaxy size-mass distribution since z = 3. *ApJ* 788, 28. doi:10.1088/0004-637X/788/1/28

van Dokkum, P. G., Franx, M., Kriek, M., Holden, B., Illingworth, G. D., Magee, D., et al. (2008). Confirmation of the remarkable compactness of massive quiescent galaxies at $z \sim 2.3$: Early-type galaxies did not form in a simple monolithic collapse. *ApJ* 677, L5–L8. doi:10.1086/587874

van Dokkum, P. G., Whitaker, K. E., Brammer, G., Franx, M., Kriek, M., Labbé, I., et al. (2010). The growth of massive galaxies since z = 2. *ApJ* 709, 1018–1041. doi:10.1088/0004-637X/709/2/1018

Vavryčuk, V. (2022a). Cosmological redshift and cosmic time dilation in the FLRW metric. *Front. Phys.* 10, 826188. doi:10.3389/fphy.2022.826188

Vavryčuk, V. (2022b). Considering light-matter interactions in Friedmann equations based on the conformal FLRW metric. *J. Adv. Res.* doi:10.1016/j.jare.2022.06.015

Verheijen, M. A. W. (2001). The Ursa Major Cluster of galaxies. V. H I rotation curve shapes and the Tully-Fisher relations. *ApJ* 563, 694–715. doi:10.1086/323887

Visser, M. (2015). Conformally Friedmann-Lemaître-Robertson-Walker cosmologies. *Class. Quantum Gravity* 32, 135007. doi:10.1088/0264-9381/32/13/135007

Weinberg, D. H., Mortonson, M. J., Eisenstein, D. J., Hirata, C., Riess, A. G., and Rozo, E. (2013). Observational probes of cosmic acceleration. *Phys. Rep.* 530, 87–255. doi:10.1016/j.physrep.2013.05.001

Weinberg, S. (1972). *Gravitation and cosmology: Principles and applications of the general theory of relativity*. New York: John Wiley & Sons.

White, S. D. M., Frenk, C. S., Davis, M., and Efstathiou, G. (1987). Clusters, filaments, and voids in a universe dominated by cold dark matter. *ApJ* 313, 505. doi:10.1086/164990

White, S. D. M., and Rees, M. J. (1978). Core condensation in heavy halos: A two-stage theory for galaxy formation and clustering. *MNRAS* 183, 341–358. doi:10.1093/mnras/183.3.341

Whitney, A., Conselice, C. J., Bhatawdekar, R., and Duncan, K. (2019). Unbiased differential size evolution and the inside-out growth of galaxies in the deep CANDELS GOODS fields at $1 \leq z \leq 7$. *ApJ* 887, 113. doi:10.3847/1538-4357/ab53d4

Williams, R. J., Quadri, R. F., Franx, M., van Dokkum, P., Toft, S., Kriek, M., et al. (2010). The evolving relations between size, mass, surface density, and star formation in 3×10^4 galaxies since z = 2. *ApJ* 713, 738–750. doi:10.1088/0004-637X/713/2/738

Windley, B. F. (1984). *The evolving continents/2nd revised and enlarged.* edition/. New York: Wiley.

Zaritsky, D., Courtois, H., Muñoz-Mateos, J. C., Sorce, J., Erroz-Ferrer, S., Comerón, S., et al. (2014). The baryonic Tully-Fisher relationship for S^4G galaxies and the "condensed" baryon fraction of galaxies. *AJ* 147, 134. doi:10.1088/0004-6256/147/6/134

Zhang, W., Li, Z., and Lei, Y. (2010). Experimental measurement of growth patterns on fossil corals: Secular variation in ancient Earth-Sun distances. *Chin. Sci. Bull.* 55, 4010–4017. doi:10.1007/s11434-010-4197-x

Zwicky, F. (1937). On the masses of nebulae and of clusters of nebulae. *ApJ* 86, 217. doi:10.1086/143864

Zwicky, F. (2009). Republication of: The redshift of extragalactic nebulae. *General Relativ. Gravit.* 41, 207–224. doi:10.1007/s10714-008-0707-4

Appendix A Gravitational orbits in the expanding Universe described by the FLRW metric

The metric tensor $g_{\mu\nu}$ of a gravitational field produced by a point mass M situated in space obeying the FLRW metric reads (Noerdlinger and Petrosian, 1971, their Eq. 11)

$$ds^2 = -c^2(1+2\alpha)\,dT^2 + a^2(T)\left((1-2\alpha)\frac{dr^2}{1-kr^2} + r^2 d\Omega^2\right), \quad \text{(A-1)}$$

where T is the proper time and

$$\alpha = -\frac{GM}{rc^2},\ |\alpha| \ll 1, \quad \text{(A-2)}$$

is the Newtonian gravitational potential normalized to c^2, and G is the gravitational constant. Assuming a massive non-relativistic particle ($v \ll c$) orbiting in the gravitational field in the plane defined by $\phi = 0$ and calculating the Christoffel symbols $\Gamma^{\mu}_{\alpha\beta}$ in the geodesic Eq. 9, we get the following approximate equations

$$\ddot{r} - r\dot{\phi}^2 - \frac{GM}{\alpha^2 r^3} + 2\frac{\dot{a}}{a}\dot{r} = 0, \quad \text{(A-3)}$$

$$r\ddot{\phi} + 2\dot{r}\dot{\phi} + \frac{\dot{a}}{a}r\dot{\phi} = 0, \quad \text{(A-4)}$$

where dots over quantities mean derivatives with respect to time T. Inserting the proper distance $R = a(T)r$ into Eq. A-3 we get

$$\ddot{R} = -\frac{GM}{R^2} + R\dot{\phi}^2 + \frac{\ddot{a}}{a}R. \quad \text{(A-5)}$$

Similarly, Eq. A-4 can be rewritten as

$$\frac{d}{dT}\left(a^2 r^2 \dot{\phi}\right) = \frac{d}{dT}\left(R^2\dot{\phi}\right) = \frac{d}{dT}L = 0, \quad \text{(A-6)}$$

where $L = RV^{\phi}$ is the proper angular momentum, and V^{ϕ} is the proper tangential velocity. Consequently, we can write (Carrera and Giulini, 2010, their Eq. 12a, b)

$$\ddot{R} = -\frac{GM}{R^2} + \frac{L^2}{R^3} + \frac{\ddot{a}}{a}R, \quad \text{(A-7)}$$

$$L = \text{const.} \quad \text{(A-8)}$$

The equations are called the modified Newtonian equations and they differ from the standard Newtonian equations describing the Kepler orbits by term $\frac{\ddot{a}}{a}R$ in Eq. A-7 related to the space expansion. The analysis of the modified Newtonian equations applied to the galaxy dynamics shows that assuming a constant L, the expansion term $\frac{\ddot{a}}{a}R$ affects the orbits within galaxies negligibly (Faraoni and Jacques, 2007).